Meteoritics & Planetary Science 39, Nr 4, 545–565 (2004)
Abstract available online at http://meteoritics.org

Spectral reflectance-compositional properties of spinels and chromites: Implications for planetary remote sensing and geothermometry

Edward A. CLOUTIS,[1] J. M. SUNSHINE,[2] and R. V. MORRIS[3]

[1]Department of Geography, University of Winnipeg, Winnipeg, Manitoba R3B 2E9, Canada
[2]Science Applications International Corporation, 4501 Daly Drive, Chantilly, Virginia 20151, USA
[3]NASA Johnson Space Center, Code SN3, 2101 NASA Road 1, Houston, Texas 77058–3696, USA
*Corresponding author. E-mail: e.cloutis@uwinnipeg.ca

(Received 29 January 2003; revision accepted 2 March 2004)

Abstract–Reflectance spectra of spinels and chromites have been studied as a function of composition. These two groups of minerals are spectrally distinct, which relates largely to differences in the types of major cations present. Both exhibit a number of absorption features in the 0.3–26 μm region that show systematic variations with composition and can be used to quantify or constrain certain compositional parameters, such as cation abundances, and site occupancies. For spinels, the best correlations exist between Fe^{2+} content and wavelength positions of the 0.46, 0.93, 2.8, Restrahelen, 12.3, 16.2, and 17.5 μm absorption features, Al and Fe^{3+} content with the wavelength position of the 0.93 μm absorption feature, and Cr content from the depth of the absorption band near 0.55 μm. For chromites, the best correlations exist between Cr content and wavelength positions of the 0.49, 0.59, 2, 17.5, and 23 μm absorption features, Fe^{2+} and Mg contents with the wavelength position of the 1.3 μm absorption feature, and Al content with the wavelength position of the 2 μm absorption feature. At shorter wavelengths, spinels and chromites are most readily distinguished by the wavelength position of the absorption band in the 2 μm region (<2.1 μm for spinels, >2.1 μm for chromite), while at longer wavelengths, spectral differences are more pronounced. The importance of being able to derive compositional information for spinels and chromites from spectral analysis stems from the relationship between composition and petrogenetic conditions (pressure, temperature, oxygen fugacity) and the widespread presence of spinels and chromites in the inner solar system. When coupled with the ability to derive compositional information for mafic silicates from spectral analysis, this opens up the possibility of deriving petrogenetic information for remote spinel- and chromite-bearing targets from analysis of their reflectance spectra.

INTRODUCTION

Spinel-group minerals, specifically spinel, hercynite, and chromite, are found in a wide range of terrestrial and extraterrestrial geological environments. The spectral reflectance properties of spinel-group minerals in the $MgAl_2O_4$-$Fe^{2+}Al_2O_4$-$Fe^{2+}Cr_2O_4$ (spinel-hercynite-chromite) compositional space have been examined in conjunction with compositional and structural information to derive systematic and quantifiable spectral-compositional relationships. Such relationships could allow the presence, abundance, and composition of these minerals to be determined from optical remote sensing data. This would enable petrogenetic conditions to be assessed for inaccessible targets such as asteroids and aid terrestrial geological exploration and mapping based on optical remote sensing of spinel-rich targets.

The spinel group of minerals is diverse and encompasses a number of common and widespread minerals, including magnetite, spinel-hercynite, and chromite. Spinels frequently accommodate extensive cation substitutions such as Fe^{2+}-Mg in spinel-hercynite, Fe^{2+}-Zn in spinel-gahnite, Al^{3+}-Cr^{3+} in spinel/hercynite-magnesiochromite/chromite, and partial Al-Fe^{3+} substitution in hercynite-magnetite (Deer et al. 1966). This complex chemistry can lead to confusion in nomenclature. This discussion focuses largely on the spinel-hercynite ($MgAl_2O_4$-$Fe^{2+}Al_2O_4$) and spinel-hercynite-magnesiochromite-chromite ([Mg, Fe^{2+}]Al_2O_4- [Mg, Fe^{2+}]Cr_2O_4) series. For the sake of clarity, Cr-rich spinels will be referred to as chromite, and Mg- and Fe^{2+}-rich aluminous spinels will be referred to as spinel.

The spectral properties of various spinel-group minerals have been examined by a number of investigators (e.g.,

Rossman 1988b, and references therein). The 0.3–3.3 μm spectra are generally characterized by a broad and intense absorption feature in the 2 μm region in the case of normal spinels (e.g., Cloutis and Gaffey 1993) or by a single broad absorption feature in the 1 μm region in the case of inverse spinels such as magnetite (e.g., Adams 1975) and by additional, less intense absorption bands at shorter wavelengths (e.g., Hunt and Wynn 1979). However, to date, no systematic studies have examined the spectral reflectance properties of spinels and chromites as a function of composition in this wavelength region. Comprehensive spectral reflectance-compositional studies can provide important insights into the causes of spectral variations and quantitative data for use in the interpretation of optical remote sensing data (e.g., Cloutis and Gaffey 1991).

The widespread presence of spinels and chromites, the relationship between composition and formation conditions, their unique spectral properties, usefulness as geothermometers and geobarometers, and the ability to apply laboratory reflectance spectra directly to the analysis of optical remote sensing data were the rationales for undertaking this study. It was felt that a systematic study of the spectral reflectance-compositional relationships of spinels and chromites would permit quantitative mapping of their abundances and compositions to be undertaken using optical remote sensing data, which, in turn, would allow geological histories and formation conditions (e.g., geothermometry, geobarometry, oxygen fugacity) of spinel- and chromite-bearing targets to be determined remotely.

IMPORTANCE OF SPINELS AND CHROMITES

Geological Exploration

Spinels and hercynites are high-formation temperature minerals most commonly found in intensely metamorphosed rocks such as granulites, alumina-rich xenoliths, and in igneous mafic and ultramafic rocks (Deer et al. 1966; Evans and Frost 1975; Allan et al. 1988; Dyar et al. 1989). Hence, spinels are not uniquely associated with any specific type of economic mineral deposit. Their presence in certain types of xenoliths, and their resistance to erosion makes them useful indicator minerals for kimberlite exploration (e.g., Rossman and Smyth 1990) and for genetic interpretation of other deposit types of potential economic importance, such as lamproites (Wagner and Velde 1987).

Chromites and chromian-spinels are commonly associated with high-temperature mafic and ultramafic occurrences. Concentrated deposits of chromite are often found in layered intrusions where this mineral is concentrated through gravity segregation and accumulation (Irvine 1975; Evans 1980). Chromites can also be concentrated in placer deposits due to their resistance to weathering and erosion. Chromite is the major source of chromium, hence, identification of chromite-rich deposits is of potential economic importance. The common association of chromite with mafic and ultramafic intrusions is also useful in the exploration for deposits of other strategic materials associated with these rock types (Evans 1980; Eckstrand 1984).

Extraterrestrial Occurrences

Spinel-hercynite is present in various classes of meteorites, most commonly in carbonaceous chondrites, particularly the CO class, where it occurs almost exclusively in calcium-aluminum inclusions (CAIs) (McSween 1977). Spinel abundances in these meteorites may reach a few wt%. These abundances are sufficient to enable their presence to be determined using reflectance spectroscopy (Rajan and Gaffey 1984; Cloutis and Gaffey 1993). Spinel is present in only a few other meteorite classes, including relatively unaltered ordinary chondrites (Bischoff and Keil 1983, 1984) and angrites (Prinz et al. 1990) at, generally, less than 1 wt% abundance.

Chromite is the most widespread spinel-group mineral found in meteorites. It is commonly present at the one to few percent level in brachinites (Prinz et al. 1986; Meteorite Working Group 1991), mesosiderites (Powell 1971), pallasites (Buseck 1977; Boesenberg et al. 1995), HED achondrites (Mason 1963; Dymek et al. 1976), and shergottites and chassignites (Mason et al. 1975; Floran et al. 1978; Smith et al. 1984). Chromite is also present at the <1% level in ordinary chondrites (Keil 1962; Dodd et al. 1967), winonaites, and lodranites (Graham et al. 1977; Prinz et al. 1978, 1980; King et al. 1981). Two meteorites are notable for their chromite contents. Elephant Moraine (EET) 84302, provisionally classified as an acapulcoite, contains 23 vol% chromite heterogeneously distributed in the meteorite (Takeda et al. 1993; Yugami et al. 1996). Lewis Cliffs (LEW) 88774 has been classified as a Cr-rich ureilite and contains 6 vol% chromite (Mikouchi et al. 1995; Chikami et al. 1997). Spinels have been found in some lunar samples, most notably dunites (Smith and Steele 1976). Spinels have also tentatively been identified in the reflectance spectra of a number of S- and K-class asteroids (Burbine et al. 1992; Hiroi et al. 1996).

Petrogenesis

Geothermometers and geobarometers involving spinels and chromites are of two broad types: those based on the presence or absence of a mineral or mineral assemblage (e.g., Gutmann 1986) and those based on compositional variations of spinels, and coexisting minerals in some cases (e.g., Jamieson and Roeder 1984). The development of widely applicable spinel geothermometers and geobarometers is somewhat hampered by the fact that spinels are subject to extensive cation substitutions. Broadly, the presence of spinels is commonly indicative of high formation or

metamorphic temperatures in meteorites (Bischoff and Keil 1983, 1984) and in primary terrestrial deposits (e.g., Deer et al. 1966; Nicholls and Carmichael 1972; Rumble 1973).

Specific petrogenetic applications of spinels that have been developed include: the temperature- and pressure-dependent solubility of Al in orthopyroxene coexisting with olivine and spinel (Macgregor 1974; Obata 1976; Danckwerth and Newton 1978; Gasparik and Newton 1984); temperature dependent Fe-Mg partitioning between coexisting olivine and spinel (Fabries 1979; Roeder et al. 1979; Sack 1982; Jamieson and Roeder 1984; Sack and Ghiorso 1991) or between coexisting pyroxene and chromite (Mukherjee et al. 1990); dependence of the pyroxene + spinel – garnet + olivine reaction boundary on pressure and Cr-Fe-Al abundances (Macgregor 1970); pressure and oxygen fugacity dependence of ferric iron content in coexisting olivine + orthopyroxene + spinel assemblages (O'Neill and Wall 1987) and in Mg-Fe spinels (Mattioli and Wood 1986, 1988); temperature dependent Al-Mg disordering and cation site occupancies in spinels (Wood et al. 1986; Nell et al. 1989); oxygen fugacity dependence of the stability field of hercynite (Woodland and Wood 1990); and cation abundance versus coexisting mineral abundances and pressure-, temperature-, and fugacity-dependent cation site occupancies in spinels and various coexisting minerals (Irvine 1965, 1967; Bunch et al. 1967; Jackson 1969; Evans and Frost 1975; Dyar et al. 1989).

EXPERIMENTAL PROCEDURE

A total of 14 naturally occurring spinel-hercynite and 9 chromite samples from various localities were included in this study. The samples consisted of single crystals, crystalline aggregates, or individual grains disseminated in rocks. Sample separates were prepared through a combination of crushing and hand picking and were examined using a microscope to remove any impurities. The samples were characterized by electron microprobe (Cloutis and Gaffey 1991), X-ray diffraction, and the Fe^{2+} and Fe^{3+} contents were determined by wet chemistry and/or Mossbauer spectroscopy. Uncertainties in composition are on the order of 0.1 wt% as oxides.

The compositions and localities of the samples are provided in Table 1 (spinels and hercynites) and Table 2 (chromites). All samples were ground to <45 μm grain size using an alumina mortar and pestle and were dry sieved for spectral measurements. Reflectance spectra were measured at the RELAB spectrometer facility at Brown University (Pieters 1983; Reflectance Experiment Laboratory 1996) at phase angles of i = 30° and e = 0° between 0.3 and 2.6 μm and i = 30° and e = 30° between 2.5 and 26 μm. The 0.3–2.6 μm spectra were measured relative to halon at 5 nm resolution. The 2.5–26 μm spectra were measured relative to brushed gold, and the spectra were merged in the 2.5–2.6 μm region. Individual spectra of these samples can be obtained from the RELAB database by searching with their designated label (e.g., CHR104) under "Sample Name." Alternatively, spectra for the group of samples can be searched using chromite as a "Subtype" and EAC as "PI." Links to the RELAB data collection can be found at http://www.planetary.brown.edu/relab.

A number of techniques were applied to analysis of the spectra. Straight line continuum removal was used to isolate absorption bands in the visible region, with the continua being tangent to the reflectance spectra on either side of the absorption features of interest. In the ensuing discussion, the wavelength positions of continuum-removed absorption bands will be referred to as band centers. Band depths were measured using Equation 32 of Clark and Roush (1984). Band minima or center wavelength positions were calculated by fitting a third order polynomial to approximately 10–20 data points located on either side of a visually determined band minimum or center. Band depths in the 2 μm region were measured using a horizontal straight line continuum tangent to the reflectance spectrum at the point of maximum reflectance, generally around 1.4 μm. Uncertainties in band positions were determined by varying the number of points used in the polynomial fitting. Spectral resolution also has an impact on the ability to precisely determine band positions. Collectively, these effects constrain the accuracy of band position determinations to ~±3 nm.

The X-ray diffraction analysis involved acquiring continuous scan data from 3–65° 2-θ on a Philips PW1710 automated powder diffractometer using a PW1050 Bragg-Brentano goniometer equipped with incident- and diffracted-beam Soller slits, 1.0° divergence and anti-scatter slits, a 0.2 mm receiving slit, and a curved graphite diffracted-beam monochromator. The normal focus Cu X-ray tube was operated at 40 kV and 40 mA using a take-off angle of 6°.

SPECTRAL PROPERTIES OF SPINELS AND CHROMITES

The spectral properties of spinels and chromites, both in transmission and reflectance, have been studied by a number of investigators, generally at wavelengths beyond 9 μm, for applications such as radiative transfer in the mantle (Shankland et al. 1974), structural elucidation (Slack et al. 1966; Dickson and Smith 1976), distinguishing natural from synthetic samples, and relating color to composition (Wood et al. 1968; Schmetzer and Gübelin 1980; Shigley and Stockton 1984; Taran et al. 1987). Spectral reflectance studies of spinels below 9 μm are more limited in scope (e.g., Slack 1964; Adams 1975). None of the existing studies provide quantitative relationships between composition and spectral reflectance variations below 9 μm.

The unit cell of spinel and chromite consists of 32 oxygen atoms and 24 cations, 8 of which are in 4-fold (tetrahedral) coordination (the A position) and 16 of which are in 6-fold (octahedral) coordination (the B position); thus, the general

Table 1. Compositions of spinel-hercynite samples used in this study.

Group	A	A	A	B	B	B	B
Sample[a]	S121	S122	S101	S116	S117	S124	S123
V_2O_5	n.d.	n.d.	0.15	0.00	0.06	0.03	0.09
SiO_2	0.00	0.00	0.38	<0.01	0.00	0.01	0.01
TiO_2	0.00	0.00	0.14	0.00	0.00	0.02	0.04
Al_2O_3	69.88	70.84	70.33	69.22	69.16	64.19	65.79
Cr_2O_3	0.19	0.25	0.41	0.00	0.15	0.03	0.10
Fe_2O_3	n.d.	n.d.	n.d.	n.d.	0.00	0.40	0.88
FeO	0.16[b]	0.22[b]	0.52[b]	2.04[b]	2.92	6.88	12.42
MnO	0.02	0.02	0.00	0.17	0.12	0.08	0.33
MgO	27.76	27.73	26.72	25.77	24.54	22.76	19.10
ZnO	0.55	0.33	1.03	1.92	2.56	1.35	0.84
CaO	0.00	0.00	0.02	<0.01	0.00	0.00	0.01
NiO	0.00	0.00	0.10	0.00	<0.01	<0.01	0.02
Na_2O	n.d.	n.d.	n.d.	0.04	0.06	0.03	0.01
Total	98.56	99.39	99.87	99.17	99.58	99.37	99.64
Group	C	C	C	D	D	D	D
Sample[a]	S115	S125	S119	S127	S114	H101	S126
V_2O_5	0.00	0.00	0.01	0.34	0.33	0.14	0.00
SiO_2	0.01	0.05	0.01	0.13	0.13	0.07	0.02
TiO_2	0.21	0.43	0.05	0.68	0.58	0.67	0.03
Al_2O_3	65.55	65.30	64.75	61.29	61.82	59.84	64.68
Cr_2O_3	0.00	0.02	0.06	0.23	0.15	0.05	0.04
Fe_2O_3	3.82	3.98	3.27	5.98	4.40	6.23	2.00
FeO	3.17	3.59	9.33	12.58	14.04	15.18	12.03
MnO	0.14	0.16	0.18	0.15	0.09	0.12	0.18
MgO	25.74	25.90	21.36	19.37	18.56	18.01	19.11
ZnO	0.08	0.05	0.92	0.14	0.14	n.d.	1.08
CaO	0.00	0.00	0.01	0.00	0.00	0.00	<0.01
NiO	0.00	<0.01	0.03	0.20	0.19	0.04	0.03
Na_2O	0.01	<0.01	0.01	0.00	0.01	0.03	0.01
Total	98.73	99.48	99.99	101.09	100.44	100.38	99.21

[a]Localities of samples: H101: Sycamore Canyon, Cochise Co., AZ, USA; S101: Salem District, Kangayam, Madras Province, India; S114: Anakie, Queensland, Australia; S115: Lyon Co., NV, USA; S116: Helena, MT, USA; S117: Limecrest, NJ, USA; S119: Parker Mine, Notre Dame de Laus, Quebec, Canada; S121: Mogok, Burma; S122: Sri Lanka; S123: Otjozondjupa region, near Otjiva, Namibia; S124: Amity, Orange Co., NY, USA; S125: Kinkaid Siding, Mineral Co., NV, USA; S126: Ambatomaninty, Madagascar; S127: Bo Phloi, Kanchoutabori Province, Thailand.
[b]All Fe reported as FeO.

Table 2. Composition of chromite samples used in this study.

Sample[a]	C101	C102	C103	C104	C105	C106	C107	C108	C109
V_2O_5	0.19	0.28	0.20	0.05	0.26	0.14	0.10	n.d.	n.d.
SiO_2	0.00	0.13	0.02	<0.01	0.02	0.06	0.01	0.01	<0.01
TiO_2	0.15	0.84	0.05	0.06	0.36	0.14	0.13	0.28	0.32
Al_2O_3	10.98	18.75	6.99	30.05	17.07	9.89	5.49	16.78	8.51
Cr_2O_3	57.56	40.98	63.10	35.80	51.28	56.66	63.99	52.06	58.84
Fe_2O_3	3.83	5.90	4.66	3.28	2.80	6.07	3.32	1.42	3.47
FeO	10.93	22.63	11.94	10.46	13.23	15.55	13.63	12.94	14.24
MnO	0.26	0.35	0.31	0.20	0.29	0.62	0.31	0.25	0.31
MgO	13.62	9.11	12.16	17.42	13.44	10.26	12.40	14.35	12.36
CaO	0.09	0.08	0.03	<0.01	<0.01	<0.01	<0.01	0.00	<0.01
NiO	0.23	0.00	0.10	0.25	0.12	0.06	0.10	0.11	0.08
Na_2O	n.d.	n.d.	0.00	0.00	0.00	0.00	0.00	0.00	<0.01
Total	97.84	99.05	99.56	97.57	98.87	99.45	99.48	98.40	98.27

[a]Localities of samples: C101: Valley Springs, Calaveras Co., CA, USA; C102: Stillwater Intrusion, MT, USA; C103: El Dorado Co., CA, USA; C104: Manila Bay, The Philippines; C105: Red Ledge Mine, Nevada Co., CA, USA; C106: Jacksonville, Tuolumne Co., CA, USA; C107: Placer Co., CA, USA; C108: San Benito Co., CA, USA; C109: El Dorado Co., CA, USA.

formula can be written as $A_8B_{16}O_{32}$ (or AB_2O_4). In normal spinel-group minerals, which include spinel, hercynite, and chromite, the A sites are ideally fully occupied by divalent cations such as Fe^{2+} and Mg^{2+}, and the B sites (which are twice as numerous as the A sites) are ideally fully occupied by trivalent cations such as Al^{3+}, Fe^{3+}, or Cr^{3+}.

Ferrous iron located in the tetrahedrally coordinated A site of spinel and chromite is the major cation that gives rise to crystal field transition absorption bands (e.g., Shankland et al. 1974; Gaffney 1973). The tetrahedral site is non-centrosymmetric so that Jahn-Teller effects cause a splitting of the energy levels of Fe^{2+}, leading to an intense crystal field absorption feature in the 2 μm region. The precise nature of this feature is not well-established. A number of previous investigators have assigned two or more distinct absorption bands to this feature (Slack 1964; Slack et al. 1966; Shankland et al. 1974), and some reflectance spectra show evidence for more than one band in the 2 μm region (Adams 1975). However, most investigators do not discriminate differences in the energy levels and assign this feature to undifferentiated Fe^{2+} crystal field transitions (Gaffney 1973; Mao and Bell 1975).

The few spinel spectra measured between 2.5 and 9 μm show an additional absorption feature near 2.8 μm that can be resolved into two distinct bands in low-temperature spectra (Slack 1964; Slack et al. 1966). This feature is also attributed to Fe^{2+} crystal field transitions, although Reed (1971) assigns it to O-H stretching vibrations involving H in the octahedral sites. Detailed analysis of this feature can be hampered by the presence of O-H stretching fundamental absorption bands in this region (Hunt 1977; Rossman and Smyth 1990). Very little H_2O or OH is required for intense bands to appear in this region, even for "anhydrous" minerals (e.g., Roush et al. 1985). Thus, the use of this wavelength region for compositional determinations needs to be approached cautiously.

Spinel and chromite spectra also exhibit additional absorption features at shorter wavelengths. These can be quite numerous in high resolution spectra and have been studied by a number of investigators (Tables 3 and 4). The assignment of these bands is somewhat complicated by the presence of multiple cations in most natural samples, and there is broad agreement on the assignments for only some of the bands.

Most spectral studies of spinels and chromites have focused on the wavelength region beyond ~9 μm (e.g., Hafner and Laves 1961; Preudhomme and Tarte 1971a, b, c, 1972; White and DeAngelis 1967; Farmer 1974). Absorption bands in this wavelength region are attributed to various stretching and bending vibrations involving the tetrahedral and octahedral cations and oxygen.

RESULTS

The spinel samples have been grouped into four groups on the basis of the Mossbauer data and similarities in their reflectance spectra (Table 1). Group A consists of the samples (SPI101, 121, 122) with low iron abundances and weak or nonexistent iron absorption bands in the 0.9 μm region. Group B also consists of low iron samples (SPI116, 117, 123, 124) but with information on the ferrous/ferric ratios (with the exception of SPI116). Group C consists of higher iron samples (SPI115, 119, 125), and Group D is the highest iron content samples (HER101, SPI114, 127) (Fig. 1). We have also included SPI126 in this latter group even though Mossbauer analysis indicates the presence of magnetite, which can lower overall reflectance and introduce additional absorption bands. The chromite spectra are shown in Fig. 2.

All of the spectra exhibit a number of absorption bands below 1 μm. In spinels, the most intense and ubiquitous of these bands appear near 0.39, 0.46, 0.55, 0.66, and 0.93 μm, broadly consistent with previous results. In chromites, the most intense and ubiquitous of these bands appear near 0.49, 0.59, 0.69, and 0.94 μm, as well as an absorption feature near 1.26 μm.

The band near 0.39 μm, which is only evident in the spinel spectra, has been assigned to either a ^5E-$^3T_1(^3G)$ tetrahedral Fe^{2+} spin-forbidden transition or a $^4A_2$-$^4T_1$ octahedral Cr^{3+} crystal field transition (Table 3). Some of the confusion in the assignment of this band may arise from its potential complexity. Sevastyanov and Orekhova (1971) found that this band consisted of two overlapping absorption features near 0.388 and 0.415 μm. Two distinct bands are resolvable in some of the continuum removed spinel spectra (Fig. 3), but in most cases, the longer wavelength band appears as a shoulder on the 0.39 μm band. Shankland et al. (1974) also suggest that the absorption feature in this region may be resolved into two absorption bands at 0.373 and 0.387 μm. Two resolvable bands were only found in the continuum removed spectrum of SPI117, although there is some evidence for a second band that appears as a shoulder on the more intense 0.39 μm feature in some of the other spinel spectra. Poole (1964), who attributed this band to Cr^{3+}, found that the wavelength position of the band increases with increasing Cr content in synthetic $Mg(Al, Cr)_2O_4$ spinels. Wood et al. (1968) found that the wavelength position of this band decreased when Zn substituted for Mg in the structure.

The spinel reflectance data show a weak positive correlation between the position of this band and its depth. Band depth is inversely correlated with Cr content but is not correlated with Fe^{2+} content. All of the spectra are <45 μm-sized samples, so grain size variations should not be a significant factor. Band position is positively correlated with Fe^{2+} content and negatively correlated with Cr content, although in all cases, there is substantial scatter in the data. Taken together, these results suggest that Fe^{2+} is the major contributor to this feature, with a probable additional contribution from Cr.

The absorption feature at 0.46 μm in the spinel spectra has been attributed by most investigators to a ^5E-$^3E(^3G)$ tetrahedral

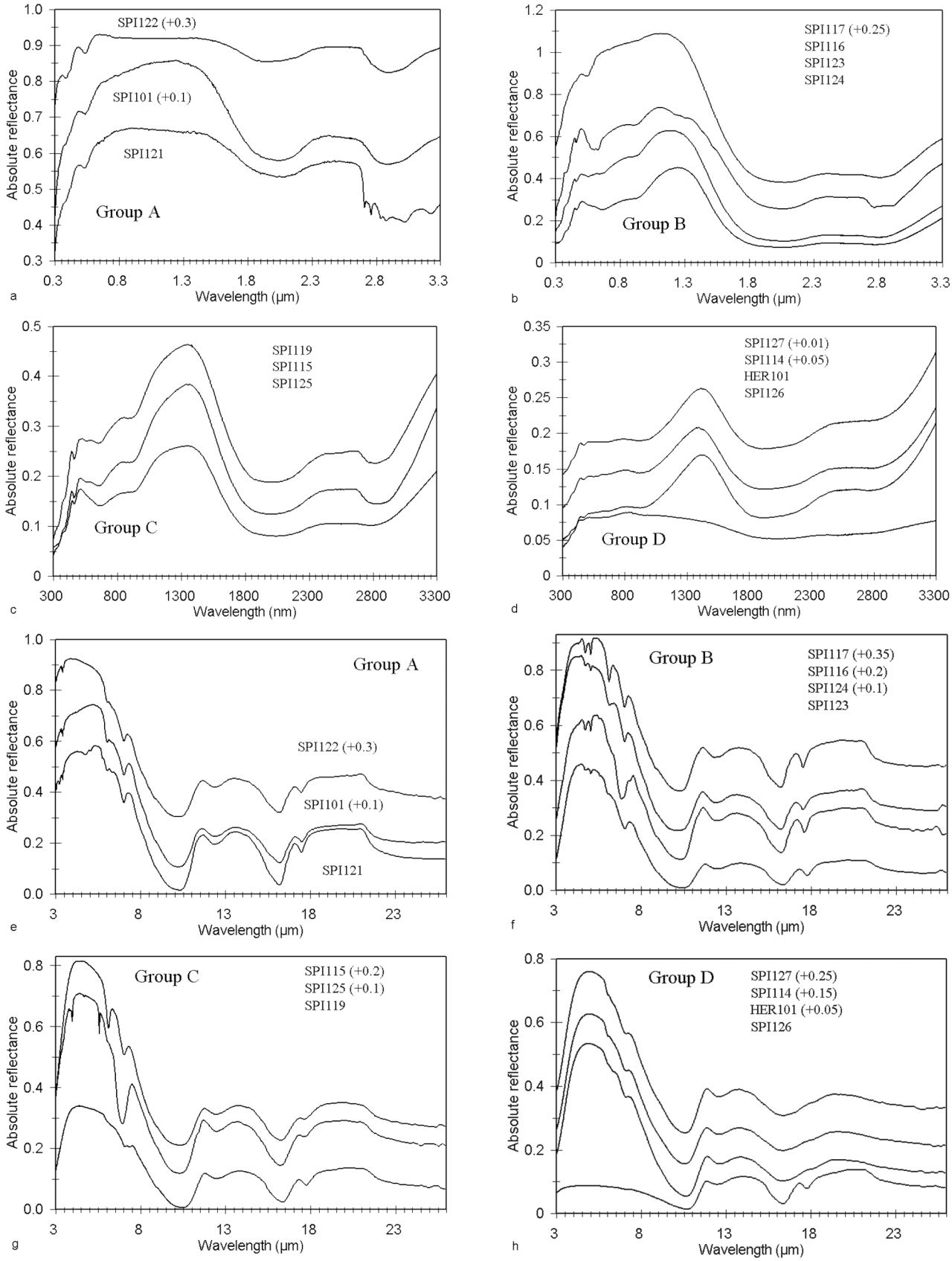

Fig. 1. Reflectance spectra (0.3–3.3 [a–d] and 3–26 μm [e–h]) of spinels used in this study (see Table 1). The order of the spectra and vertical offsets are indicated on the figure.

Table 3. Absorption band assignments in the visible and near-infrared regions of Al-spinels (where Al >Cr) from previous investigators. The most intense bands are indicated in bold.

Position (μm)	Cation[a]	Position (μm)	Cation[a]	Position (μm)	Cation[a]	Source of data[b]
0.459	Fe^{2+}	0.552	Fe^{2+}	0.557	Fe^{2+}	
0.592	Fe^{2+}					1
0.366	Fe^{2+} tet.	**0.383**	Fe^{2+} tet.	0.455	Fe^{2+} tet.	
0.476	Fe^{2+} tet.	0.506	Fe^{2+} tet.	**0.554**	Fe^{2+} tet.	
0.578	unknown	**0.633**	unknown	0.661	unknown	
0.903	Fe^{2+} oct.					2
0.354	Fe^{2+} tet.	0.370	Fe^{2+} tet.	0.385	Fe^{2+} tet.	
0.458	Fe^{2+} tet.	0.467	Fe^{2+} tet.	0.510	Fe^{2+} tet.	
0.552	Fe^{2+} tet.	0.70	Fe^{2+} tet.			3
0.642	Fe^{2+} tet.	0.662	Fe^{2+} tet.	0.682	Fe^{2+} tet.	4
0.388–0410	Cr^{3+} oct.	0.540–0.560	Cr^{3+} oct.			5
0.418	Cr^{3+} oct.	0.575	Cr^{3+} oct.			6
0.490	Fe^{2+}	0.540	Cr^{3+}	0.559	V^{3+}	
0.571	Fe^{2+}					7
0.325	Cr^{3+} oct.	**0.390**	Cr^{3+} oct.	0.440	Cr^{3+} oct.	
0.550	Cr^{3+} oct.					8
0.372	Fe^{2+} tet.	0.374	Fe^{2+} tet.	0.388	Fe^{2+} tet.	9
0.430	Fe	0.434	Fe	**0.460**	Fe	
0.480	Co	0.510	Fe	0.544	Co	
0.552	Fe	**0.559**	Fe	**0.575**	Co/Fe	
0.595	Co/Fe	**0.622**	Co/Fe			10
0.335	Cr^{3+} oct.	0.370	Cr^{3+} oct.	0.455	Cr^{3+} oct.	
0.467	Cr^{3+} oct.	0.516	Cr^{3+} oct.	0.550	Cr^{3+} oct.	
0.553	Cr^{3+} oct.	0.655	Cr^{3+} oct.	0.750	Cr^{3+} oct.	
0.924	Fe^{3+} tet.					11
0.325	Cr^{3+} oct.	0.391	Cr^{3+} oct.	0.439	Cr^{3+} oct.	
0.550	Cr^{3+} oct.					12
0.461–0.469	Fe^{2+} tet.	0.476	Fe^{2+} tet.	0.556	Fe^{2+} tet.	
0.575–0.592	Fe^{2+} tet.	0.637	Fe^{2+}-Fe^{3+}	0.658–0.667	Fe^{2+}-Fe^{3+}	
0.901	Fe^{2+} tet.					13
0.433		0.443		0.458	Fe^{2+}	
0.508		0.540	Cr	0.555		
0.585		0.635				14
0.388	Cr^{3+} oct.	0.415	Cr^{3+} oct.	0.540	Cr^{3+} oct.	15

[a]tet. = tetrahedrally coordinated cation; oct. = octahedrally coordinated cation.

[b]Source of data: 1 = Anderson and Payne (1937): natural blue spinels; 2 = Dickson and Smith (1976): natural spinel; 3 = Gaffney (1973): re-examination of spectra of Slack (1964) for a natural and synthetic spine; 4 = Mao and Bell (1975): natural lunar spinel; 5 = Poole (1964): synthetic and natural spinels; 6 = Reed (1971): synthetic Cr-doped $MgAl_2O_4$; 7 = Schmetzer and Gübelin (1980): natural spinel; 8 = Sevastyanov and Orekhova (1971): synthetic Cr-doped $MgAl_2O_4$; 9 = Shankland et al. (1974): one natural spinel; 10 = Shigley and Stockton (1984): synthetic (Co-doped) and natural blue spinels; 11 = Slack (1964): synthetic and natural spinels; 12 = Sviridov et al. (1973): "magnesium spinel;" 13 = Taran et al. (1987): seven natural spinels; 14 = Webster (1983): natural spinels; and 15 = Wood et al. (1968): natural spinels.

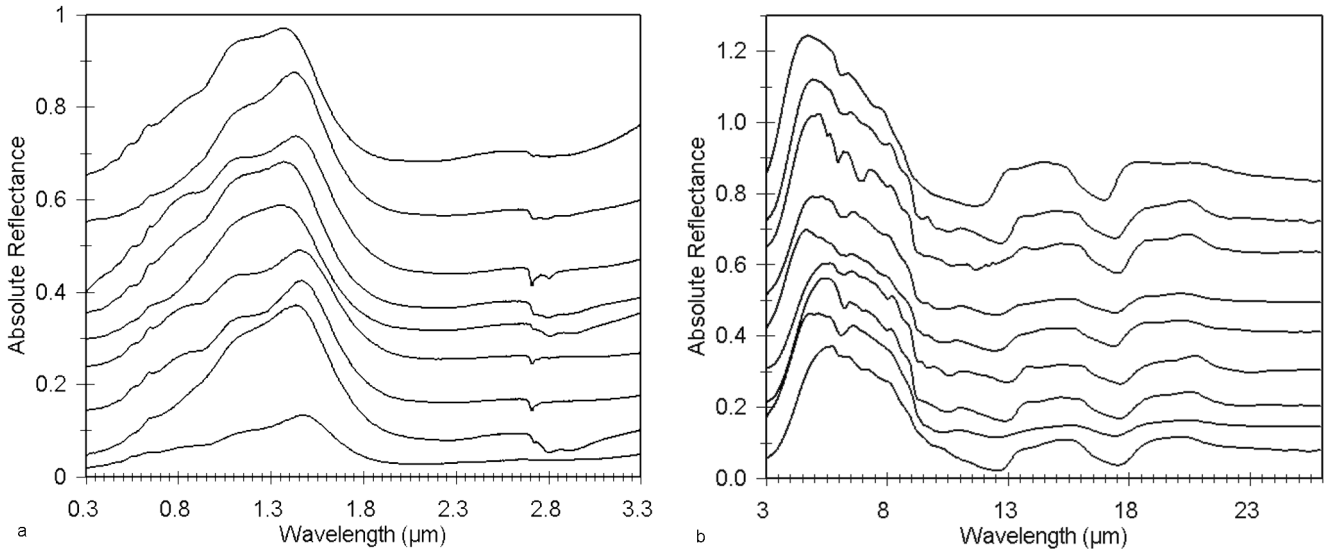

Fig. 2. Reflectance spectra (0.3–3.3 [a] and 3–26 μm [b]) of the chromites (see Table 2). The spectra have been stacked in order of increasing iron content from bottom to top (with one exception) and vertically offset for clarity. The amount of vertical offset and order of the spectra from bottom to top is as follows: (a) CHR102 (–0.02) (this sample is not in the sequence of increasing iron content used for the other spectra); CHR106 (+0.0); CHR109 (+0.1); CHR107 (+0.2); CHR105 (+0.25); CHR108 (+0.3); CHR103 (+0.35); CHR101 (+0.5); CHR104 (+0.6). (b) CHR102 (no offset); CHR106 (+0.1); CHR109 (+0.15); CHR107 (+0.25); CHR105 (+0.35); CHR108 (+0.45); CHR103 (+0.55); CHR101 (+0.65); CHR104 (+0.75).

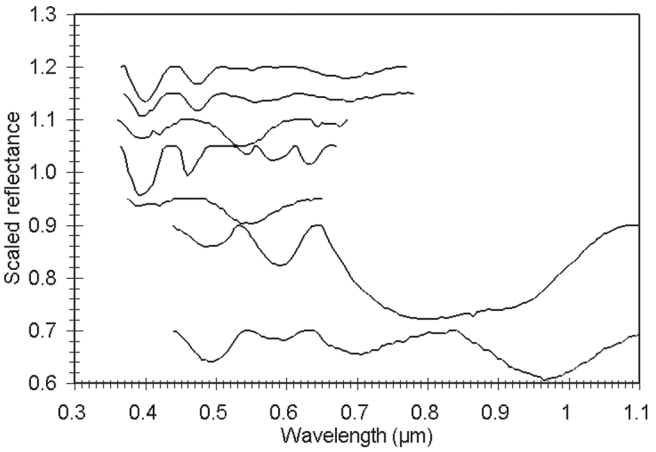

Fig. 3. Reflectance spectra of some of the spinel and chromite spectra after division of a series of straight line continua tangent to the reflectance spectra on either side of some of the absorption features. Spectra have been vertically offset for clarity as follows (from top to bottom): HER101 (+0.20); SPI114 (+0.15); SPI121 (+0.10); SPI116 (+0.05); SPI101 (no offset); CHR101 (–0.10); CHR102 (–0.30).

Fe^{2+} spin-forbidden transition (Table 3). There is a weak positive correlation between band depth and band position. There is no apparent correlation between Fe^{2+} content and band depth, and there is a weak negative correlation with Cr content. Band center position is not correlated with Cr content but does show a positive correlation with Fe^{2+} content, as expected. However, there is some scatter in the data, such that the wavelength position of this band can only be used to constrain FeO content above ~10 wt% to within ~±2% FeO (Fig. 4). The various band assignments, useful correlation ranges, and accuracies are summarized in Table 6.

The absorption band located near 0.49 μm in chromites is probably attributable to a $^4A_2$-$^4T_1$ crystal field transition in octahedrally coordinated Cr^{3+} (Table 4). There are no strong correlations between band depth and either Fe^{2+} or Cr content, but the band center position is positively correlated with Cr content, suggesting that this assignment is correct. It can generally be used to constrain Cr_2O_3 content to within approximately ±5% (Fig. 5). This band appears to consist of two partially overlapped bands located near 0.48 and 0.49 μm in a number of the chromite spectra (Fig. 3; bottom two spectra); this may account for some of the scatter in the data.

The assignment of the absorption feature near 0.55 μm in spinels has been variously assigned to either a ^5E-$^3T_1(^3H)$ tetrahedral Fe^{2+} spin-forbidden transition or a $^4A_2$-$^4T_2$ octahedral Cr^{3+} crystal field transition (Table 3). There is no correlation between band center position and depth. However, we did find a generally negative correlation between band depth and Fe^{2+} content and a weak positive correlation with Cr content, suggesting that this band is attributable to Cr. The band center position was not strongly correlated with either Fe^{2+} or Cr content, contrary to the results of Poole (1964), who found a positive correlation between band position and Cr content in synthetic $Mg(Al, Cr)_2O_4$ spinels. Many of the spinel spectra exhibit complex absorptions in the 0.53–0.58 μm region of the continuum-removed spectra, showing either two partially resolved absorption bands or an asymmetric absorption feature in this region (Fig. 3).

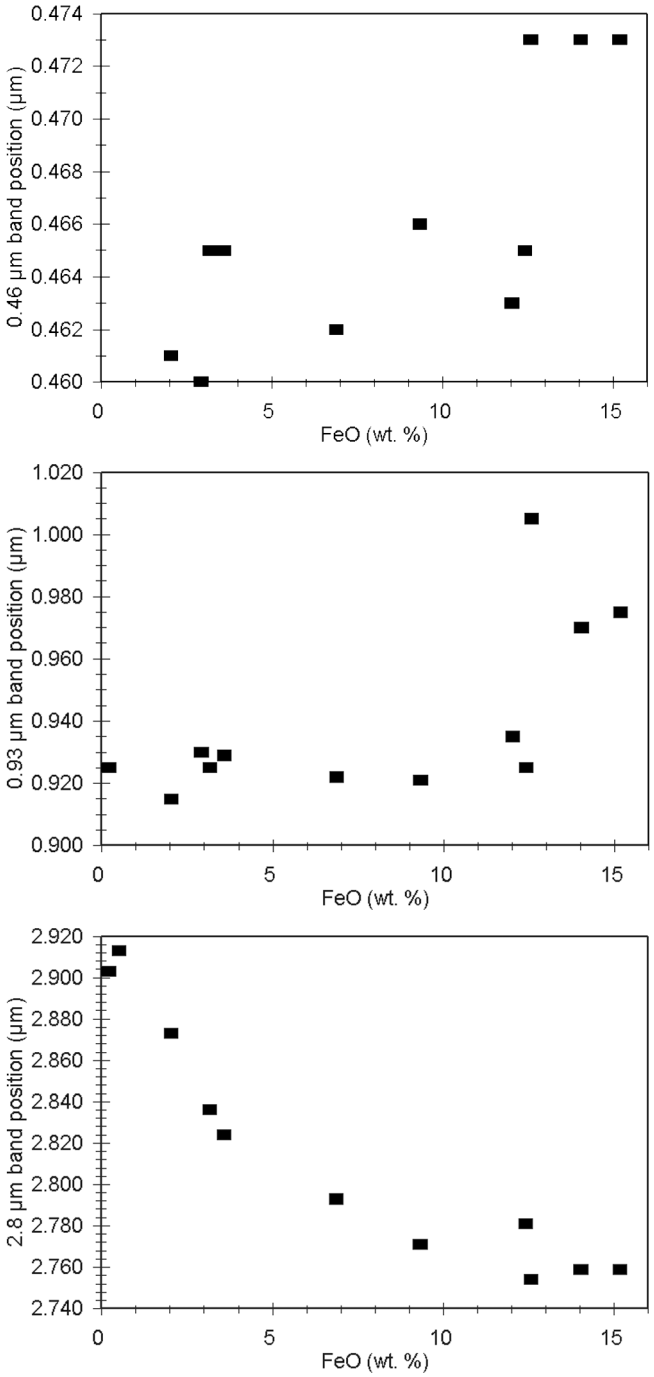

Fig. 4. FeO content of spinels versus wavelength positions of 0.46 µm absorption band center (top), 0.93 µm absorption band center (middle), and 2.8 µm absorption band minimum.

Collectively, these results suggest that both cations contribute to this absorption feature.

The absorption feature located near 0.59 µm in chromites has been attributed to a $^4A_2$-$^4T_2$ crystal field transition in octahedrally coordinated Cr^{3+} (Table 4). Both band depth and band center position are positively correlated with Cr content, and the latter seems particularly useful for quantifying Cr content, generally to within ±2 wt% Cr_2O_3 (Fig. 5).

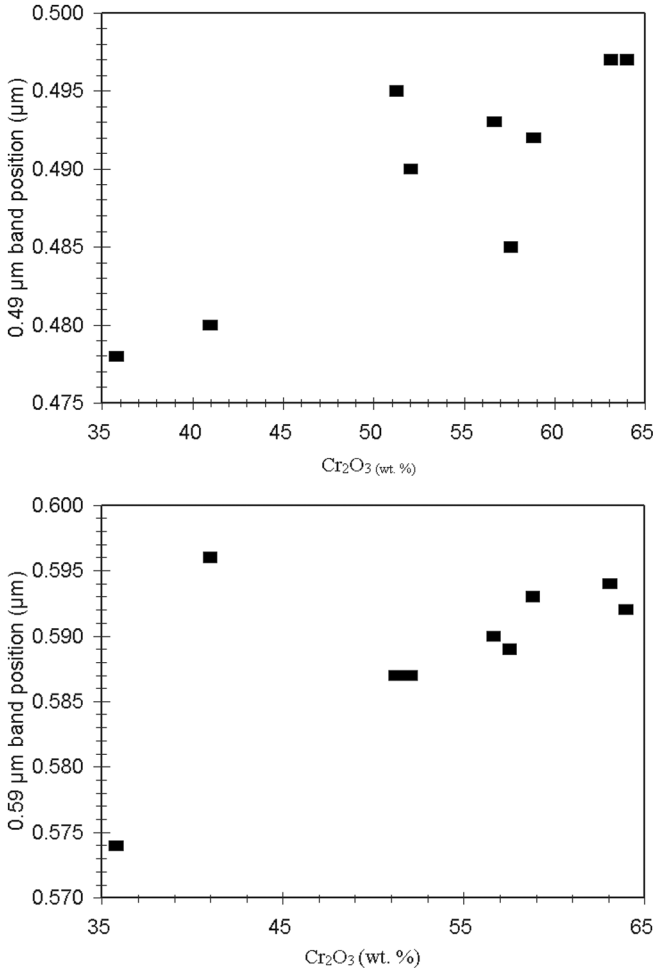

Fig. 5. Cr_2O_3 content of chromites versus wavelength positions of the 0.49 µm (top) and 0.59 µm (bottom) absorption band centers.

The absorption feature present near 0.66 µm in spinel spectra is variously attributed to a ^5E-^3T tetrahedral Fe^{2+} spin-forbidden transition, a $^4A_2$-$^2E(^2G)/^2T_1(^2G)$ crystal field transition in octahedrally coordinated Cr^{3+}, or an Fe^{2+}-Fe^{3+} intervalence charge transfer (Table 3). Many of the spinel spectra show complex absorption features in this region (Fig. 3). There is no apparent correlation between band depth and band center position. Neither band depths nor band centers are strongly correlated with Cr, Fe^{2+}, Fe^{3+}, or total Fe content. These observations all suggest that absorptions in this region are probably attributable to both Fe and Cr, and the lack of correlations probably arises from overlapping multiple absorption bands, which cannot be well-resolved given the spectral resolution of the data (5 nm).

The absorption feature near 0.69 µm in chromite spectra is attributed to a ^5E-$^3T_1$ tetrahedral Fe^{2+} spin-forbidden transition (Table 4). Only six of the chromite spectra exhibit a resolvable absorption band in this region, and all of these show an additional band in the 0.66 µm region, similar to that seen in the spinel spectra. No useful correlations emerge between band depths and positions and either Cr or Fe^{2+} content from

Table 4. Absorption band assignments in the visible and near-infrared regions of chromites (where Cr >Al) from previous investigators.

Position (μm)	Cation[a]	Position (μm)	Cation[a]	Position (μm)	Cation[a]	Source of data[b]
0.426	Cr^{3+} oct.	0.592	Cr^{3+} oct.			1
0.424	Cr^{3+} oct.	0.575	Cr^{3+} oct.	1.500	Cr^{2+} tet.	2
~0.65	Cr^{3+} oct.					3
0.450	Cr^{3+} oct.	0.530	Cr^{3+} oct.	0.656	Fe^{3+} tet.	
0.660	Cr^{3+} oct.	0.682	Fe^{2+} tet.	0.950	Fe^{2+} oct.	
1.30	Cr^{2+} tet.					4
0.418–0.426	Cr^{3+} oct.	0.576–0.583	Cr^{3+} oct.			5
0.37	Cr^{3+} oct.	~0.49	Cr^{3+} oct.	0.58	Cr^{3+} oct.	
1.0–1.05	Fe^{2+} oct.	~1.1–1.3	Cr^{2+} tet.			6

[a]tet. = tetrahedrally coordinated cation; oct. = octahedrally coordinated cation.

[b]Source of data: 1 = Burns and Vaughan (1975): natural picrochromite ($MgCr_2O_4$); 2 = Greskovich and Stubican (1966): synthetic (Mg, Cr^{2+})Cr_2O_4; 3 = Hunt and Wynn (1979): natural chromite; 4 = Mao and Bell (1975): three natural chromites (1 annealed); 5 = Poole (1964) synthetic and natural picrochromites; 6 = Ulmer and White (1966): synthetic chromites.

Table 5. Derived spectral-compositional trends for spinels and chromites.

Absorption band	Correlation	Useful range	Average accuracy
Spinels			
0.46 μm band position	Positive with FeO	10–15% FeO	±2% FeO
0.93 μm band position	Positive with FeO	10–15% FeO	±2% FeO
0.93 μm band position	Negative with Al_2O_3	57–66% Al_2O_3	±2% Al_2O_3
0.93 μm band position	Positive with Fe_2O_3	0–7% Fe_2O_3	±1% Fe_2O_3
0.93 μm band depth	Negative with Al_2O_3	57–66% Al_2O_3	±2% Al_2O_3
2.8 μm band position	Negative with FeO	0–16% FeO	±1% FeO
Restrahlen position	Positive with FeO	0–16% FeO	±1% FeO
12.3 μm band position	Positive with FeO	0–16% FeO	±2% FeO
16.2 μm band position	Positive with FeO	0–16% FeO	±1% FeO
17.5 μm band position	Positive with FeO	0–16% FeO	±1% FeO
Chromites			
0.49 μm band position	Positive with Cr_2O_3	35–65% Cr_2O_3	±4% Cr_2O_3
0.59 μm band position	Positive with Cr_2O_3	35–65% Cr_2O_3	±2% Cr_2O_3
1.3 μm band position	Positive with FeO	10–23% FeO	±1% FeO
1.3 μm band position	Negative with MgO	9–18% MgO	±2% MgO
2 μm band position	Negative with Al_2O_3	5–30% Al_2O_3	±3% Al_2O_3
2 μm band position	Positive with Cr_2O_3	35–65% Cr_2O_3	±3% Cr_2O_3
2 μm band position	Positive with YCr	0.5–0.9 YCr	±0.4 YCr
Restrahlen position	Positive with Cr_2O_3	35–65% Cr_2O_3	±5% Cr_2O_3
17.5 μm band position	Positive with Cr_2O_3	35–65% Cr_2O_3	±4% Cr_2O_3
23 μm band position	Negative with Cr_2O_3	35–65% Cr_2O_3	±4% Cr_2O_3

this limited data set. These results support the assignment of this band to Fe^{2+} but do not provide enough data points to construct a reliable spectral-compositional relationship.

The higher iron content spinels and all the chromite spectra exhibit an absorption feature in the 0.93 μm region, probably attributable to a spin-allowed $^5T_2$-^5E crystal field transitions in Fe^{2+} located in the octahedral site (Mao and Bell 1975). While site occupancies of Fe^{2+} were not determined for our samples, the compositional data provide some validation of this assignment. Band depths for the spinels are negatively correlated with Al content (Fig. 6), consistent with the fact that Al has a higher octahedral site preference than Fe^{2+} (Navrotsky and Kleppa 1967). It appears that band depth increases rapidly when Al_2O_3 content falls below ~63 wt%, suggesting that decreasing Al content is correlated with increasing Fe^{2+} octahedral site occupancy.

The wavelength position of the 0.93 μm band center in the spinels is relatively constant (~0.927 μm) up to ~13 wt%

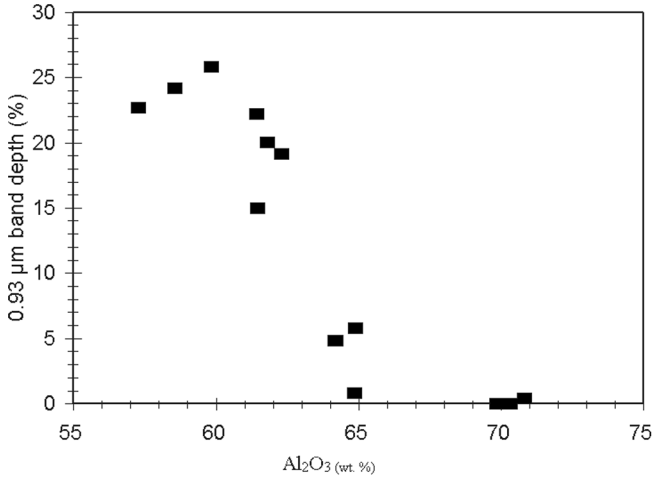

Fig. 6. Depth of the 0.93 µm band versus Al_2O_3 content for the spinels.

FeO, beyond which it seems to shift to longer wavelengths (Fig. 4). It is also negatively correlated with Al content and positively correlated with Fe_2O_3 content (Fig. 7). The fact that a correlation exists with cations other than Fe^{2+} suggests that cation substitutions change the local electronic environment around octahedrally coordinated Fe^{2+} cations sufficient to cause spectrally detectable changes in site configuration. The distribution of the data points is again suggestive of a non-linear correlation; such non-linearities between composition and band positions have been found for other minerals (e.g., Cloutis and Gaffey 1991).

Chromite spectra exhibit an absorption band near 1.3 µm, which is not seen in spinel spectra. This band is attributed to a spin-allowed $^5T_2$-^5E crystal field transition in Cr^{2+} located in the tetrahedral site (Table 4). Interestingly, this band shows an increase in wavelength position with increasing Fe^{2+} content and decreasing MgO content (Fig. 8) and only a weak positive correlation with total Cr content. The former relationship may be due to Cr^{2+} preferentially occupying the tetrahedral site at the expense of Fe^{2+}. We cannot definitively determine this, as the oxidation state and site occupancies of the chromium in our samples was not determined. Greskovich and Stubican (1966) found that the wavelength position of this band moves to shorter wavelengths with increasing tetrahedrally coordinated Cr^{2+} in a series of synthetic (Mg, Cr^{2+})Cr_2O_4 spinels; they attributed this shift to site distortions accompanying cation substitutions. The current data suggest that the wavelength position of this band can be used to constrain chromite FeO and MgO contents to within ±2% over the compositional ranges examined (Table 6).

The absorption feature located near 2 µm, found in both spinel and chromite spectra, is extremely broad and more intense than the shorter wavelength bands. It is attributed to a ^5E-$^5T_2$ crystal field transition in tetrahedrally coordinated Fe^{2+}. The distortion of this site leads to very intense absorption (Slack et al. 1966; Mao and Bell 1975; Burns 1993). As a result, band depths increase rapidly with increasing Fe^{2+} content and can exceed 80% with as little as 3 wt% FeO.

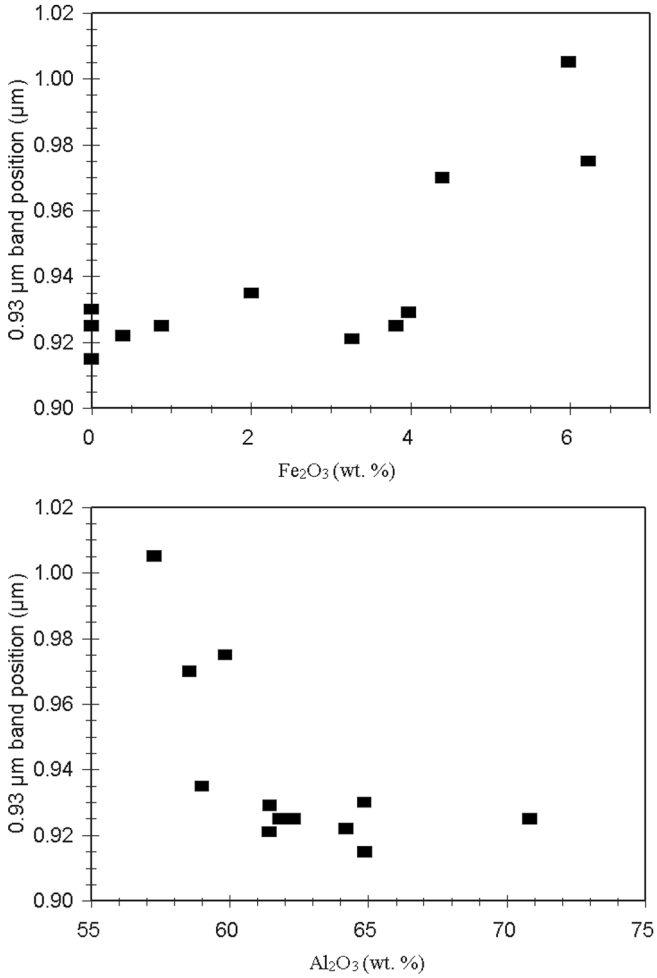

Fig. 7. Wavelength position of the 0.93 µm continuum removed band center of the spinels versus Fe_2O_3 (top) and Al_2O_3 (bottom) contents.

The wavelength position of the minimum reflectance of this feature shows no well-defined trend with Fe^{2+} content for either the spinels or chromites, although there is a weak negative correlation with Fe^{3+} content for the spinels. It should also be noted that there is no systematic relationship between Fe^{2+} and Fe^{3+} content for the samples nor is a correlation expected. The lack of correlation between band position and Fe^{2+} content may be due to differences in the relative proportions of tetrahedral and octahedral Fe^{2+}. Another possibility is that the various cation substitutions which characterize spinel cause its structure and, hence, tetrahedral electronic environment to vary in complex ways. A third explanation is that this feature consists of more than one highly overlapped band due to Jahn-Teller splitting of the Fe^{2+} orbitals (Slack et al. 1966; Shankland et al. 1974) and that each band may respond in different ways to increasing Fe^{2+} content, effectively obscuring any systematic trends that may be present for an individual band.

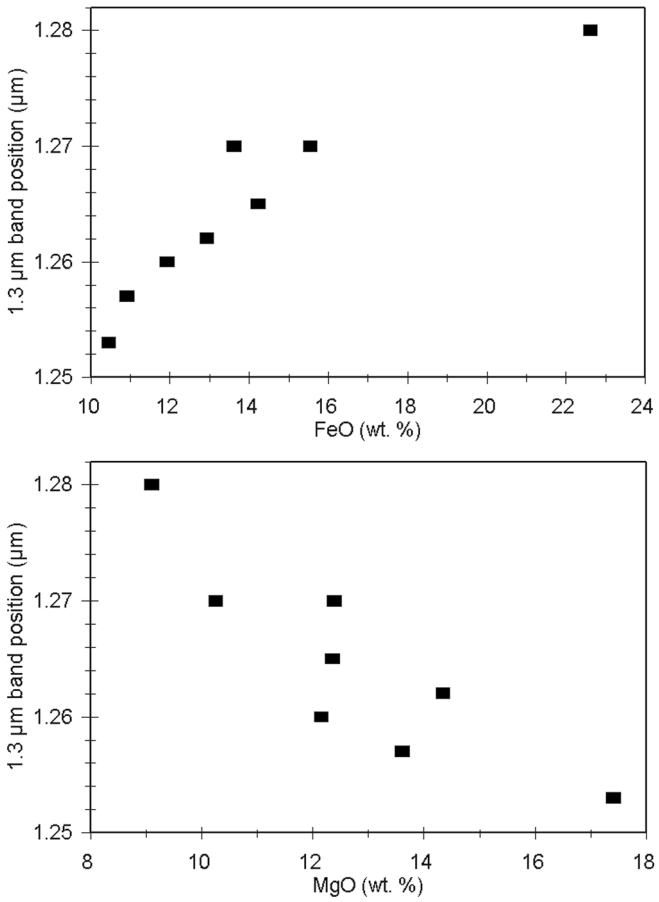

Fig. 8. Wavelength position of the 1.3 µm band center versus FeO (top) and MgO (bottom) contents for the chromites.

The wavelength position of the 2 µm feature in the chromite spectra shows a positive correlation with Cr content and the $Cr_2O_3/(Cr_2O_3 + Al_2O_3 + Fe_2O_3)$ ratio and a negative correlation with Al content (Fig. 9). This is not unexpected, as Al and Cr commonly substitute for one another. While this feature is attributable to Fe^{2+} crystal field transitions, the correlation with Cr content is probably valid because each oxygen in a spinel structure is shared between one tetrahedral and three octahedral cations. Thus, as Cr substitutes for Al in the transition from spinel to chromite, oxygen-cation bond lengths may change, resulting in changes in absorption band wavelength positions (Preudhomme and Tarte 1971a, b; Farmer 1974).

There is also a clear separation between the chromites and spinels in terms of band minima wavelength position; it always occurs shortward of 2.1 µm in the spinel spectra and longward of 2.1 µm in the chromite spectra. This separation is again probably attributable to the interactions between the octahedral and tetrahedral cations through their shared oxygens (Farmer 1974). Thus, it appears that the wavelength position of this band can be used to rapidly discriminate Mg-Fe spinels from chromites.

All the spectra exhibit an absorption feature near 2.8 µm,

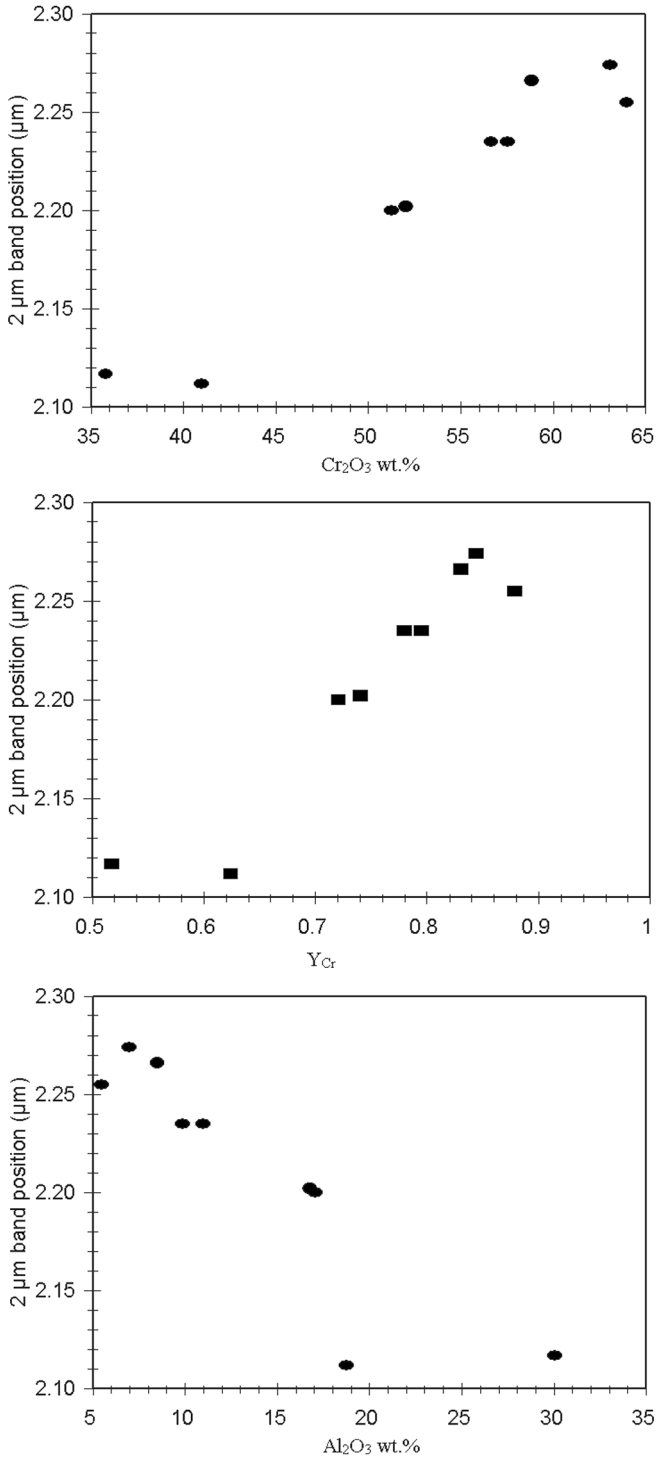

Fig. 9. Wavelength position of the 2 µm band minimum versus Cr_2O_3 content (top), Y_{Cr} content (middle), and Al_2O_3 content (bottom) for the chromites.

the nature of which has not been intensively investigated in previous studies. This is largely due to the fact that it occurs near the wavelength position of the intense O-H stretching fundamentals (e.g., Reed 1971; Rossman 1988a). Some investigators have suggested that this band appears to be

largely attributable to Fe^{2+} crystal field transitions (e.g., Rossman and Smyth 1990) and likely consists of two overlapped bands (Slack et al. 1966). A number of lines of evidence suggest that this band is attributable to Fe^{2+} crystal field transitions rather than O-H stretching. Its wavelength position is negatively correlated with Fe^{2+} content (Fig. 4) in the spinels. This trend is sufficiently constrained to allow derivation of Fe^{2+} content to within ±1 wt% FeO. No systematic trends were found for this band with Fe^{2+} or Cr^{3+} content in the chromites.

The alternative explanation is that the 2.8 μm absorption feature is attributable to O-H stretching associated with H situated in the octahedral sites (Reed 1971). If this band were due to O-H stretches, we would expect its wavelength position to be fairly invariant, particularly given the small amounts of H that the spinel structure can actually accommodate (Rossman and Smyth 1990); we would also not expect to find the strong negative correlation between band position and Fe^{2+} content (Reed 1971). A number of the spinel and chromite spectra exhibit sharp O-H stretching fundamental bands superimposed on this broad absorption band near 2.8 μm.

Beyond 3 μm, the spinel and chromite reflectance spectra exhibit a number of additional absorption features. The most prominent of these are present near 10.3, 12.3, 16.2, and 17.5 μm in spinels and near 10, 12.5, 17.5, and 23 μm in chromites. Previous investigators have encountered some difficulties in assigning precise mechanisms to these features because of the complex stretching and bending metal-oxygen vibrations that these minerals can undergo. This arises from the fact that each oxygen atom in the normal spinel structure is bound to one tetrahedral and three octahedral cations (Preudhomme and Tarte 1971c). There is a general consensus, however, that the major absorption bands in the 9–26 μm region arise from metal-oxygen stretching vibrations, while bending vibrations generally occur beyond ~20 μm (White and DeAngelis 1967; Preudhomme and Tarte 1971c; Farmer 1974; Estep-Barnes 1977). There are four infrared active stretching vibrations (ν_1, ν_2, ν_3, ν_4) in spinel-group minerals.

On the basis of previous transmission spectral studies of spinels, we assign the absorption band near 10.3 μm to the Restrahlen feature. The position of this band moves to longer wavelengths with increasing iron content (Fig. 10). Although only three stretching metal-oxygen bands are predicted in the 9–25 μm region, additional bands can arise due to ordering of cations on tetrahedral or octahedral sites or by structural distortions. The ν_1 and ν_2 bands are the most asymmetric and strongest bands in transmission spectra. On the basis of these previous investigations and observations, we assign the feature at 12.3 μm to ν_1, the 16.2 μm feature to ν_2, and the 17.5 μm feature to ν_3. Previous investigators have found varying degrees of correlation between the wavelength positions of these bands and compositional parameters such as tetrahedral and octahedral cation sizes and abundances (e.g., Preudhomme and Tarte 1971c). In our samples, all of these bands move to longer wavelengths with increasing ferrous iron content (the most variable cation in our samples) (Fig. 10).

A similar situation exists for chromites. The chromite spectra are generally more complex than the spinel spectra in the 9–26 μm region, probably due to the fact that extensive substitutions exist for both the tetrahedral (Mg and Fe^{2+}) and octahedral cations (Al, Cr, Fe^{3+}) in our samples. Once again, the most intense feature is the Restrahlen feature near 12 μm, which generally moves to longer wavelengths with increasing Cr content (Fig. 11). Absorption features in the 10 μm region are complex, and band positions do not exhibit any clear trends with composition. The ν_1, ν_2, and ν_3 stretching vibrations are assigned to the features near 17.5 μm, 19.5 μm, and 23 μm, respectively. The more complex absorption feature near 10 μm is assigned to a combination of the $\nu_2 + \nu_3$ bands. The absorption features in the 17.5 and 23 μm regions do exhibit some correlation with Cr content (Fig. 11).

APPLICATIONS TO PETROGENESIS

Spinel group minerals are widely used as indicators of petrogenesis. Jamieson and Roeder (1984) investigated the partitioning of Mg and Fe^{2+} between olivine and spinel for its use in geothermometry. They found that the distribution coefficient is close to 1 at 1300 °C and varies between 0.94 and 1.23. Thus, the composition of one phase can be constrained from a knowledge of the other; this would be particularly useful where the spectral signature of only one of the two phases of interest can be derived.

Both spinels (this study) and olivines (King and Ridley 1987) show systematic variations in Fe^{2+} absorption band wavelength positions as a function of $Mg/(Mg + Fe^{2+})$. The wavelength regions of their absorption bands are widely separate (~1 μm for olivine, ~2 μm for spinel) so that there are no interfering overlaps. Thus, once the presence of olivine and spinel are established in a reflectance spectrum, the $Mg/(Mg + Fe^{2+})$ content of one can be constrained from this value for the other given the partitioning relationship determined by Jamieson and Roeder (1984). This is particularly important in cases where the 1 μm or 2 μm regions of a spectrum may be obscured by other phases. The fact that olivine and chromite are spectrally distinct allows even small abundances of chromites to be detected in olivine-rich assemblages. Figure 12 shows the spectral changes that accompany the addition of a small amount (5 wt%) of chromite to olivine; the wavelength positions of both the olivine 1 μm and chromite 2 μm bands are unchanged in the mixture; the high reflectance of olivine in the 2 μm region allows even small abundances of chromite to be spectrally detectable.

Bunch et al. (1967) examined the chromites in a suite of ordinary chondrites. They found correlations between olivine and chromite compositions that could be used to discriminate different ordinary chondrite classes (LL, L, H) and

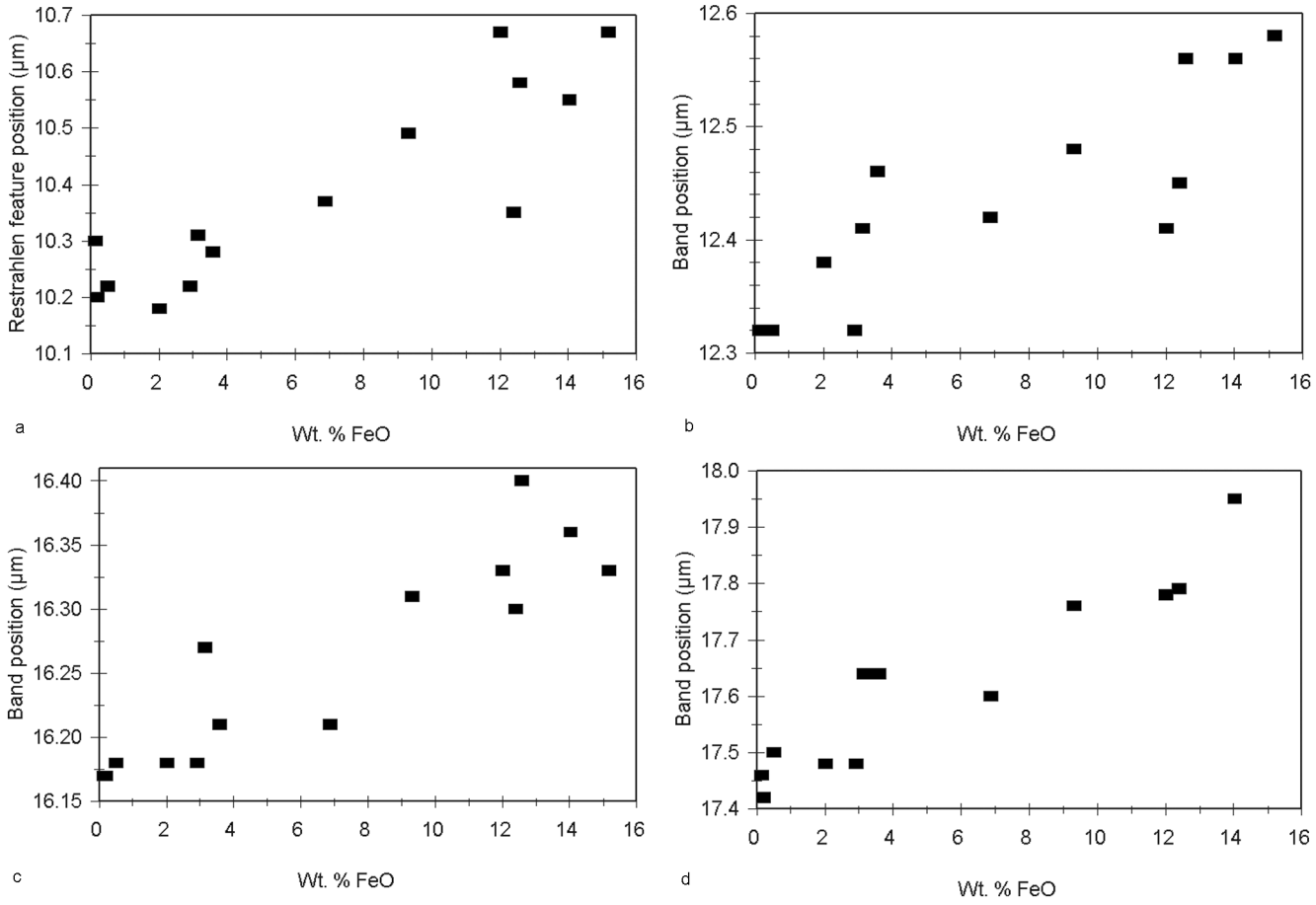

Fig. 10. FeO content versus wavelength position of the Restrahlen feature (a), 12.3 μm (b), 16.2 μm (c), and 17.5 μm (d) absorption features in spinels.

differences in petrographic subgroup. From the perspective of this study, since both olivine composition (FeO/[FeO + MgO]) (King and Ridley 1987) and chromite Cr_2O_3 content (Fig. 9) are derivable from absorption band wavelength positions, spectral information can be used to assign ordinary chondrites to their specific groups (Fig. 13). Similarly, the Cr_2O_3 content of ordinary chondrite chromite is found to correlate with petrographic grade, with Cr_2O_3 content generally decreasing with increasing petrographic grade. Consequently, both the class and petrographic grade of an ordinary chondrite are potentially derivable from analysis of the chromite spectra. Contours of absorption band positions for both chromite as a function of Cr_2O_3 content and olivine as a function of FeO content can be superimposed with the information concerning ordinary chondrite classes to develop a procedure for assigning meteorites to specific classes on the basis of the spectral-compositional properties of olivine and chromite. While such an approach to ordinary chondrite classification is obviously more laborious than established petrographic methods, it does illustrate the potential of spectroscopic analysis for providing information on petrogenetic properties of various targets. A significant complication to the use of this procedure is that the presence of pyroxene in ordinary chondrites will cause the absorption band wavelength positions of both the olivine and chromite to shift to generally shorter wavelengths (Cloutis et al. 1986); thus, extraction or isolation of the olivine and chromite, or the use of more sophisticated spectral analysis procedures, would need to be employed for this method to be effective.

The partition coefficient of Mg and Fe^{2+} in coexisting olivine and chromite can be used as a geothermometer (e.g., Evans and Frost 1975; Fabries 1979; Roeder et al. 1979). For olivine, Fe^{2+} and Mg are the major cations; Fe^{2+} content is directly derivable from spectral analysis (King and Ridley 1987), while Mg content can be reasonably approximated as 1-Fe^{2+}. In the case of the chromites, both Fe^{2+} and Mg contents are correlated with the wavelength position of the absorption band near 1.3 μm (Fig. 8). Consequently, the terms in the partition coefficient, K_D, for both olivine (OL) and chromite (CR) ($K_D = [X_{Mg}^{OL}X_{Fe}^{CR}]/[X_{Fe}^{OL}X_{Mg}^{CR}]$) can be constrained from spectral analysis. The remaining parameter that must be defined is the Cr content of chromite (Y_{Cr}); this is derivable from the wavelength position of the band near 2 μm (Fig. 9). As a result, this geothermometer could

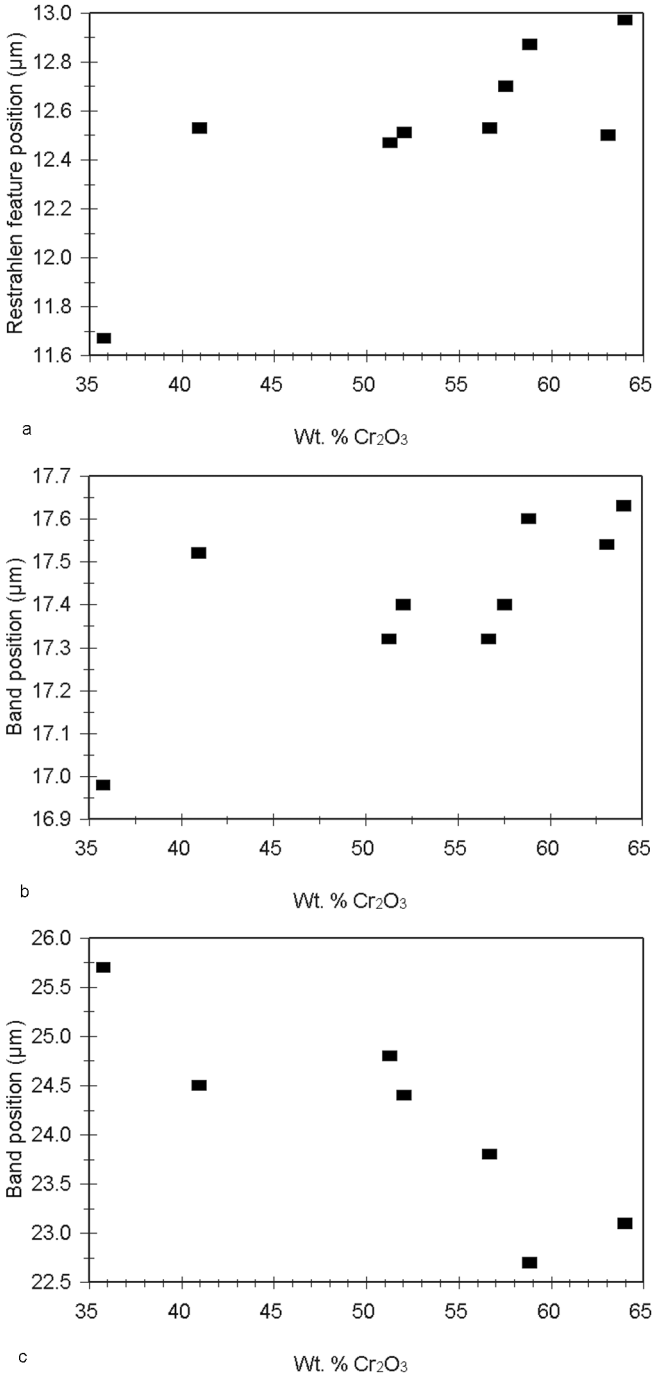

Fig. 11. Cr_2O_3 content versus wavelength position of the Restrahlen feature (a), 17.5 μm (b), and 23 μm (c) absorption features in chromites.

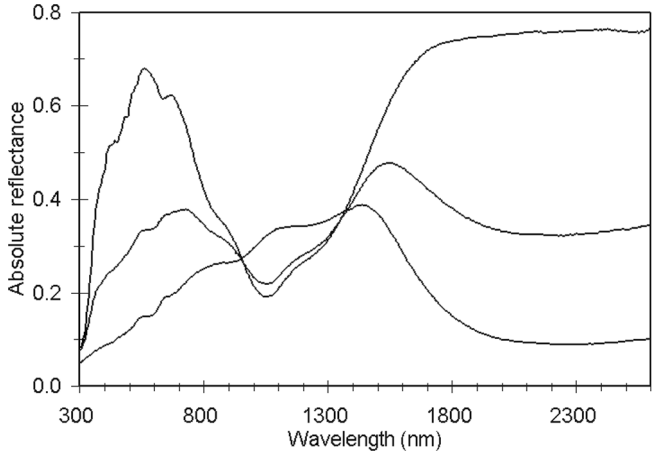

Fig. 12. Reflectance spectra of 45–90 μm-sized olivine (Fa_{11}), <45 μm-size chromite CHR103, and an intimate mixture of 95% of the olivine and 5% of the chromite. The mixture spectrum is in the middle at all wavelengths. Olivine is the highest spectrum outside the 1 μm region (lowest in the 1 μm region).

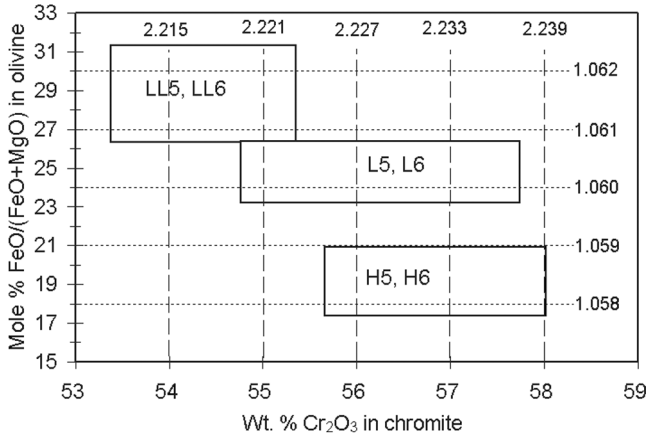

Fig. 13. Relationship of ordinary chondrite classes to Cr_2O_3 content of their chromites and FeO content of their olivine. The rectangles define the regions occupied by the various meteorite classes. The vertical and horizontal dashed lines indicate wavelength positions (in μm) of the major chromite absorption band in the 2 μm region as a function of Cr_2O_3 content and the major 1 μm region olivine absorption feature as a function of FeO content, respectively. By determining the wavelength positions of these two bands and their intersection point in the field, the type of ordinary chondrite can be determined. See text for details.

potentially be applied to remote sensing data of olivine + chromite-bearing targets. Figure 14 shows the application of the derived spectral parameters to this geothermometer. The four parameters required to calculate K_D are available from the various spectral-compositional correlations discussed above. The derived K_D value will define a horizontal line in the field of Fig. 14. The chromite Cr content will define a vertical line in the field. The intersection of these two spectrally derivable parameters will intersect with a geotherm, thereby providing information on formation temperature. The limitations and use of this geothermometer and data for various terrestrial rocks can be found in Evans and Frost (1975).

A combination of both composition and abundance of coexisting olivine and chromite can also be used to constrain formation temperatures. Useful geothermometers have been constructed based on the Mg and Fe^{2+} content of chromite and

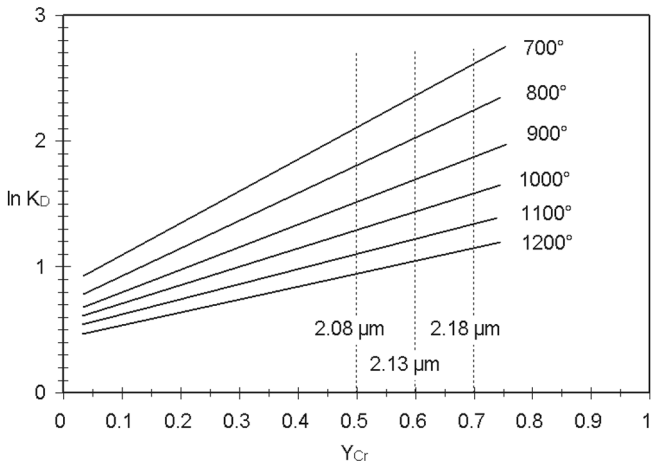

Fig. 14. Composition of coexisting olivine (OL) and chromite (CR) as a function of temperature. K_D is the distribution of Mg and Fe^{2+} in these minerals ($K_D = [X_{Mg}^{OL}X_{Fe}^{CR}]/[X_{Fe}^{OL}X_{Mg}^{CR}]$). Y_{CR} is the molar abundance of Cr in the chromite ($Y_{Cr} = Cr/[Cr + Al + Fe^{3+}]$). Spectral-compositional relationships can be used to derive both K_D and Y_{Cr}. The solid diagonal lines are geotherms (°C) (Evans and Frost 1975; Fabriès 1979). The vertical dashed lines indicate the wavelength position (in µm) of the chromite band in the 2 µm region as a function of Cr content. See text for details.

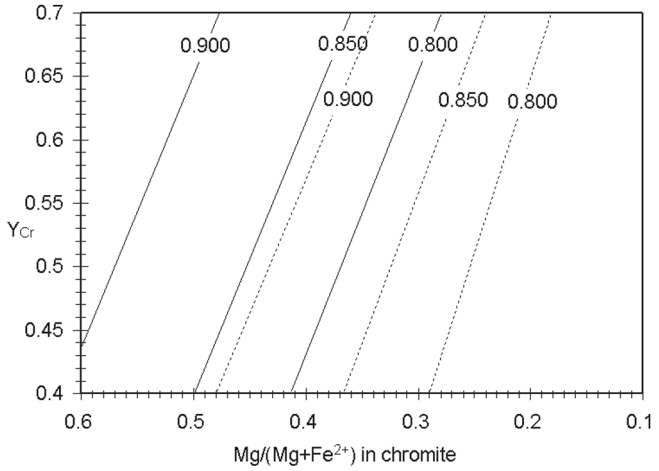

Fig. 15. Compositions of olivines and co-existing chromites for chromitites from Jackson (1969). The formation temperature can be constrained from the Mg content of the olivine (diagonal solid and dashed lines) and the Mg and Cr contents of the coexisting chromite (horizontal and vertical axes, respectively), all of which are derivable from spectral analysis. The use of this figure is described in the text.

olivine and other cations in chromite, such as Al or Cr (e.g., Jackson 1969). As was the case above, the compositional information required for most of these geothermometers is derivable from the reflectance spectra of the constituent minerals. One of the Jackson (1969) geothermometers is shown in Fig. 15. The relationship between the partitioning of Mg and Fe^{2+} between olivine and chromite is temperature dependent. Two sets of compositional isotherms are shown in the compositional space projection, for 1280 °C (solid diagonal lines) and 1000 °C (dashed diagonal lines). To calculate the formation temperature, the $Mg/(Mg + Fe^{2+})$ ratio of the olivine must be known, and this is derivable from the wavelength position of the 1 µm absorption feature of olivine (King and Ridley 1987). Various $Mg/(Mg + Fe^{2+})$ values are indicated for the two sets of isotherms in Fig. 15. This value determines which set of Mg-Fe^{2+} equipotentials to use (diagonal lines in Fig. 15). The $Mg/(Mg + Fe^{2+})$ ratio of the chromite is derivable from the chromite spectra (wavelength position of the 1.3 µm absorption feature). This constrains the compositional space along the horizontal axis. The Cr content of the chromite can also be determined spectrally from the wavelength position of the 2 µm absorption feature of chromite (Fig. 9). This constrains the compositional space along the vertical axis. With these constraints on the vertical and horizontal axes, and a knowledge of the $Mg/(Mg + Fe^{2+})$ ratio for the olivine, the formation temperature can be constrained on the basis of which isotherm for a particular $Mg/(Mg + Fe^{2+})$ ratio in olivine falls closest to the intersection of the x- and y-axis values. The units of the x- and y-axes could be changed to reflect band positions of the relevant absorption features rather than compositional parameters. Similar geotherms are available for other cations in chromite (Jackson 1969). The major limitation in the use of this geothermometer is the fact that the 1.3 µm chromite band is overlapped by the long wavelength olivine absorption band in this region (Fig. 12).

One of the most widely used geothermometers is based on the solubility of Al in orthopyroxene coexisting with olivine and spinel (Macgregor 1974; Obata 1976; Danckwerth and Newton 1978; Gasparik and Newton 1984). While this geothermometer does not rely on analysis of spinel spectral features, being able to detect the presence of spinels in such an assemblage is essential for its successful application. While the spectral properties of orthopyroxene + spinel have not been investigated, the best method for detecting spinel may be searching for the presence of a 0.49 µm spinel band, perhaps in combination with the 2.8 µm band. This is because the intense 2 µm spinel band may be overlapped by a pyroxene absorption band in the same region. The orthopyroxene Al content may be derivable from the wavelength position of the pyroxene 1 µm band, although this relationship has not been quantified (Cloutis and Gaffey 1991).

Macgregor (1970, 1974) examined the reaction of pyroxene + spinel – garnet + olivine. He found that the reaction boundary is affected by factors such as the types of pyroxenes present, their CaO content, and Cr, Al, and Fe^{3+} contents of the spinels and garnets. These compositional variations can have a significant impact on the pressure at which this reaction proceeds. Given that Fe^{3+}, Cr, and Al contents in at least some of the relevant mineral phases can be derived from spectral analysis (e.g., Cloutis and Gaffey 1991), the possibility of deriving geobarometric information from spectral analysis of relevant mineral assemblages exists.

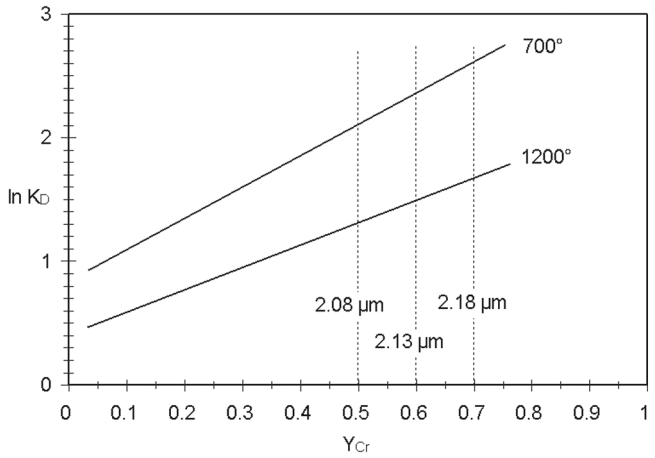

Fig. 16. Composition of coexisting orthopyroxene (OPX) and chromite (CR) as a function of temperature. K_D is the distribution of Mg and Fe^{2+} in these minerals ($K_D = [X_{Mg}^{OPX}X_{Fe}^{CR}]/[X_{Fe}^{OPX}X_{Mg}^{CR}]$). Y_{Cr} is the molar abundance of Cr in the chromite ($Y_{Cr} = Cr/[Cr + Al + Fe^{3+}]$). Spectral-compositional relationships can be used to derive both K_D and Y_{Cr}. The solid diagonal lines are geotherms (°C) (Mukherjee et al. 1990). The vertical dashed lines indicate the wavelength position (in µm) of the chromite band in the 2 µm region as a function of Cr content. See text for details.

Mukherjee et al. (1990) developed a geothermometer based on the partitioning of Mg and Fe^{2+} in coexisting orthopyroxene and chromite and the Cr content of the chromite (Fig. 16). The parameters are similar to those used for the spinel-olivine geothermometer (see above). In this case, K_D involves Mg and Fe^{2+} partitioning between coexisting orthopyroxene (OPX) and chromite (CR) ($K_D = [X_{Mg}^{OPX}X_{Fe}^{CR}]/[X_{Fe}^{OPX}X_{Mg}^{CR}]$). Orthopyroxene Fe^{2+} and Mg contents are derivable from the wavelength positions of the Fe^{2+} crystal field transition bands located near 1 and 2 µm (Cloutis and Gaffey 1991). As was the case for the olivine-spinel geothermometer above, the chromite Fe^{2+}, Mg, and Cr contents are derivable from their effects on the chromite spectra, and this geothermometer is potentially accessible with data derived solely from reflectance spectra of appropriate targets. The method of application and limitations are the same as those outlined for the olivine-chromite geothermometer above; these are also discussed in greater detail in Mukherjee et al. (1990).

Geobarometry, thermobarometry, and oxygen fugacity determinations for spinel-bearing assemblages (e.g., O'Neill and Wall 1987) are based on the oxidation state of iron in the various coexisting minerals. Determining these petrogenetic factors relies on knowledge of some combination of Fe^{2+} and Fe^{3+} contents of chromite, Fe^{2+} and Mg content of olivine and pyroxene, and cation site occupancies for the various minerals (e.g., Irvine 1965; O'Neill and Wall 1987; Mattioli and Wood 1988; Sack and Ghiorso 1991). As discussed above, most of these parameters are potentially derivable from analysis of the reflectance spectra of the relevant minerals.

Due to the fact that oxygen fugacity is interwoven throughout spinel compositional space (e.g., Irvine 1965), graphical representations of spectral-compositional relationships relevant to geobarometry and oxygen fugacity determinations can become complex. However, it is worth noting that many of the relevant compositional parameters required for such determinations are now potentially derivable by spectral analysis of the relevant mineral phases: pyroxene (Cloutis and Gaffey 1991), olivine (King and Ridley 1987), and spinels/chromites (this study). Extension of this work to more complex petrogenetic indicators based on cation site occupancies (e.g., O'Neill and Navrotsky 1984; Murck and Campbell 1986; Nell et al. 1989; Nell and Wood 1991) are potentially also derivable given that spectral features are a function of cation type and site occupancy, among other factors. However, a detailed examination of this issue is beyond the scope of this study, as the current analytical data are not adequate for this purpose.

That multiple petrogenetic indicators can be addressed through spectral analysis is also noteworthy. As an example, the geothermometers of Evans and Frost (1975) and Roeder (1979) can be used to constrain formation temperatures for a chromite-bearing assemblage (from spectral analysis). If temperature can be constrained, it is then possible to use the oxidation state of the iron in the chromite (also derivable from spectral analysis) to constrain oxygen fugacity using the relationships determined by Murck and Campbell (1986).

DISCUSSION AND CONCLUSIONS

Spinels and chromites exhibit a large number of absorption features in the 0.3–3.0 µm region associated with various transition series elements. Many of these bands are unique to either spinel or chromite, with the exception of the intense Fe^{2+} absorption bands in the 2 µm region, which is common to both minerals. In some cases, additional elemental abundances can be determined either on the basis of how elemental substitutions affect site symmetry or with some simplifying assumptions concerning composition and elemental substitutions. A number of these absorption features exhibit changes in depth and wavelength position as a function of these compositional variations.

The most highly correlated spectral-compositional parameters allow the major cation abundances in both spinels and chromites to be constrained. In the case of spinels, Fe^{2+} content is best derived from the wavelength position of the 0.46, 0.93, 2.8, 12.3, 16.2, 17.5 µm absorption bands and Restrahlen feature, and Al and Fe^{3+} contents are best derived from the wavelength position of the 0.93 µm absorption band. For chromites, Cr content is best derived from the wavelength position of the 0.49, 0.59, 2, 17.5, and 23 µm absorption bands, Fe^{2+} and Mg contents from the wavelength position of the 1.3 µm absorption band, and Al content from the wavelength position of the 2 µm absorption band. The wavelength position of the intense Fe^{2+} tetrahedrally

coordinated band in the 2 μm region can be used to rapidly separate spinels from chromites as it always occurs longward of 2.1 μm in our chromites and always shortward of 2.1 μm in our spinels. The absorption band in the 2.8 μm region is probably associated with Fe^{2+} crystal field transitions. However, this band occurs in the same region as O-H stretching fundamentals and should be used with caution. Some of the absorption bands, particularly those in the 2 and 2.8 μm region, are intense enough that spinel abundances on the order of a few wt% could be spectrally detectable.

Geothermometers, geobarometers, and measures of oxygen fugacity are related to variations in the composition and/or abundance of spinels and coexisting minerals, particularly mafic silicates such as olivine and pyroxene. When coupled with the ability to derive relevant compositional information for these mafic silicates (e.g., King and Ridley 1987; Cloutis and Gaffey 1991), petrogenetic properties of spinel-bearing assemblages can be derived from spectral analysis. With the availability of optical remote sensing data for such assemblages with sufficient spectral resolution and wavelength coverage, the possibility exists to derive enough mineralogical information to allow petrogenetic conditions to be constrained. Spinel- and chromite-associated absorption features have been detected in the reflectance spectra of calcium-aluminum inclusions from carbonaceous chondrites, a primitive achondrite, and possibly some K-class asteroids. The possibility exists that spinel and chromite absorption features are present in some asteroid and lunar spectra, but resolving this issue requires the development of more robust continuum removal procedures. Nevertheless, given the widespread presence of spinels and chromites in the inner solar system, the possibility of using spectral features associated with these phases to detect them and to conduct remote geothermometry and geobarometry is attainable.

Acknowledgments–This study was supported by a research contract from the Canadian Space Agency Space Science Program, a research grant from the Natural Sciences and Engineering Research Council, and a discretionary grant from the University of Winnipeg (all to E. A. Cloutis). We wish to thank Drs. Takahiro Hiroi and Carlé Pieters for generously providing access to the NASA-supported RELAB facility at Brown University for the spectral measurements and spectra of EET 84302. Thanks also to Trevor Mueller for his assistance with the spectral analysis and to Dr. Frank Hawthorne and Mr. Neil Ball of the Department of Geological Sciences at the University of Manitoba for acquisition of the X-ray diffraction data for the samples. Finally, thanks also to Tom Burbine and Faith Vilas for their many useful comments and suggestions for improvements and clarifications.

Editorial Handling—Dr. Carlé Pieters

REFERENCES

Adams J. B. 1975. Interpretation of visible and near-infrared diffuse reflectance spectra of pyroxenes and other rock-forming minerals. In *Infrared and Raman spectroscopy of lunar and terrestrial minerals,* edited by Karr C., Jr. New York: Academic Press. pp. 91–116.

Allan J. F., Sack R. O., and Batiza R. 1988. Cr-rich spinels as petrogenetic indicators: MORB-type lavas from the Lamont seamount chain, eastern Pacific. *American Mineralogist* 73:741–753.

Anderson B. W. and Payne C. J. 1937. Magnesium-zinc spinels from Ceylon. *Mineralogical Magazine* 24:547–554.

Bischoff A. and Keil K. 1983. Ca-Al-rich chondrules and inclusions in ordinary chondrites. *Nature* 303:588–592.

Bischoff A. and Keil K. 1984. Al-rich objects in ordinary chondrites: Related origin of carbonaceous and ordinary chondrites and their constituents. *Geochimica et Cosmochimica Acta* 48:693–709.

Boesenberg J. S., Prinz M., Weisberg M. K., Davis A. M., Clayton R. N., Mayeda T. K., and Wasson J. T. 1995. Pyroxene pallasites: A new pallasite grouplet. *Meteoritics* 30:488–489.

Bunch T. E., Keil K., and Snetsinger K. G. 1967. Chromite composition in relation to chemistry and texture of ordinary chondrites. *Geochimica et Cosmochimica Acta* 31:1569–1582.

Burbine T. H., Gaffey M. J., and Bell J. F. 1992. S-asteroid 387 Aquitania and 980 Anacostia: Possible fragments of the breakup of a spinel-bearing parent body with CO3/CV3 affinities. *Meteoritics* 27:424–434.

Burns R. G. 1993. *Mineralogical applications of crystal field theory, Second edition.* Cambridge: Cambridge University Press.

Burns R. G. and Vaughan D. J. 1975. Polarized electronic spectra. In *Infrared and Raman spectroscopy of lunar and terrestrial minerals,* edited by C. Karr, Jr. New York: Academic Press. pp. 39–72.

Buseck P. R. 1977. Pallasite meteorites: Mineralogy, petrology, and geochemistry. *Geochimica et Cosmochimica Acta* 41:711–740.

Chikami J., Mikouchi T., Takeda H., and Miyamoto M. 1997. Mineralogy and cooling history of the calcium-aluminum-chromium enriched ureilite, Lewis Cliffs 88774. *Meteoritics & Planetary Science* 32:343–348.

Clark R. N. and Roush T. L. 1984. Reflectance spectroscopy: Quantitative analysis techniques for remote sensing applications. *Journal of Geophysical Research* 89:6329–6340.

Cloutis E. A. and Gaffey M. J. 1991. Pyroxene spectroscopy revisited: Spectral-compositional correlations and relationship to geothermometry. *Journal of Geophysical Research* 96:22809–22826.

Cloutis E. A. and Gaffey M. J. 1993. The constituent minerals in calcium-aluminum inclusions: Spectral reflectance properties and implications for CO carbonaceous chondrites and asteroids. *Icarus* 105:568–579.

Cloutis E. A., Gaffey M. J., Jackowski T. L., and Reed K. L. 1986. Calibrations of phase abundance, composition, and particle size distribution for olivine-orthopyroxene mixtures from reflectance spectra. *Journal of Geophysical Research* 91:11641–11653.

Danckwerth P. A. and Newton R. C. 1978. Experimental determination of the spinel peridotite to garnet peridotite reaction in the system MgO-Al_2O_3-SiO_2 in the range 900°–1100 °C and Al_2O_3 isopleths of enstatite in the spinel field. *Contributions to Mineralogy and Petrology* 66:189–201.

Deer W. A., Howie R. A., and Zussman J. 1966. *An introduction to the rock-forming minerals.* New York: Wiley.

De Grave E. and Van Alboom A. 1991. Evaluation of ferrous and ferric Mössbauer fractions. *Physics and Chemistry of Minerals* 18:337–342.

Dickson B. L. and Smith G. 1976. Low-temperature optical absorption and Mössbauer spectra of staurolite and spinel. *The Canadian Mineralogist* 14:206–215.

Dodd R. T., Jr., Van Schmus W. R., and Koffman D. M. 1967. A survey of the unequilibrated ordinary chondrites. *Geochimica et Cosmochimica Acta* 31:921–951.

Dyar M. D., McGuire A. V., and Ziegler R. D. 1989. Redox equilibria and crystal chemistry of coexisting minerals from spinel lherzolite mantle xenoliths. *American Mineralogist* 74:969–980.

Dymek R. F., Albee A. L., Chodos A. A., and Wasserburg G. J. 1976. Petrography of isotopically-dated clasts in the Kapoeta howardite and petrologic constraints on the evolution of its parent body. *Geochimica et Cosmochimica Acta* 40:1115–1130.

Eckstrand O. R., editor. 1984. *Canadian mineral deposit types: A geological synopsis.* Economic Geology Report 36. Ottawa: Geological Survey of Canada.

Estep-Barnes P. A. 1977. Infrared spectroscopy. In *Physical methods in determinative mineralogy, Second edition,* edited by Zussman J. New York: Academic Press. pp. 529–603.

Evans A. M. 1980. *An introduction to ore geology.* London: Blackwell.

Evans B. W. and Frost B. R. 1975. Chrome-spinel in progressive metamorphism: A preliminary analysis. *Geochimica et Cosmochimica Acta* 39:959–972.

Fabriès J. 1979. Spinel-olivine geothermometry in peridotites from ultramafic complexes. *Contributions to Mineralogy and Petrology* 69:329–336.

Farmer V. C. 1974. The anhydrous oxide minerals. In *The infrared spectra of minerals,* edited by Farmer V. C. London: Mineralogical Society. pp. 183–204.

Floran R. J., Prinz M., Hlava P. F., Keil K., Nehru C. E., and Hinthorne J. R. 1978. The Chassigny meteorite: A cumulate dunite with hydrous amphibole-bearing melt inclusions. *Geochimica et Cosmochimica Acta* 42:1213–1229.

Gaffney E. S. 1973. Spectra of tetrahedral Fe^{2+} in $MgAl_2O_4$. *Physical Review B* 8:3484–3486.

Gasparik T. and Newton R. C. 1984. The reversed alumina contents of orthopyroxene in equilibrium with spinel and forsterite in the system MgO-Al_2O_3-SiO_2. *Contributions to Mineralogy and Petrology* 85:186–196.

Graham A. L., Easton A. J., and Hutchison R. 1977. Forsterite chondrites: The meteorites Kakangari, Mount Morris (Wisconsin), Pontlyfni, and Winona. *Mineralogical Magazine* 41:201–210.

Greskovich G. and Stubican V. S. 1966. Divalent chromium in magnesium-chromium spinels. *Journal of Physics and Chemistry of Solids* 27:1379–1384.

Gutmann J. T. 1986. Origin of four- and five-phase ultramafic xenoliths from Sonora, Mexico. *American Mineralogist* 71: 1076–1084.

Hafner S. and Laves F. 1961. Ordnung/Unordnung und Ultrarotabsorption III. Die Systeme $MgAl_2O_4$-Al_2O_3 und $MgAl_2O_4$-$LiAl_5O_8$. *Zeitschrift fur Kristallographie* 115:321–330.

Hiroi T., Vilas F., and Sunshine J. M. 1996. Discovery and analysis of minor absorption bands in S-asteroid visible reflectance spectra. *Icarus* 119:202–208.

Hunt G. R. 1977. Spectral signatures of particulate minerals in the visible and near infrared. *Geophysics* 42:501–513.

Hunt G. R. and Wynn J. C. 1979. Visible and near-infrared spectra of rocks from chromium-rich areas. *Geophysics* 44:820–825.

Irvine T. N. 1965. Chromian spinel as a petrogenetic indicator, Part 1. Theory. *Canadian Journal of Earth Sciences* 2:648–671.

Irvine T. N. 1967. Chromian spinel as a petrogenetic indicator, Part 2. Petrologic applications. *Canadian Journal of Earth Sciences* 4: 71–103.

Irvine T. N. 1975. Crystallization sequences in the Muskox intrusion and other layered intrusions: II. Origin of chromitite layers and similar deposits of other magmatic ores. *Geochimica et Cosmochimica Acta* 39:991–1020.

Jackson E. D. 1969. Chemical variations in coexisting chromite and olivine in chromitite zones of the Stillwater complex. *Economic Geology Monographs* 4:41–71.

Jamieson H. E. and Roeder P. L. 1984. The distribution of Mg and Fe^{2+} between olivine and spinel at 1300 °C. *American Mineralogist* 69:283–291.

Keil K. 1962. On the phase composition of meteorites. *Journal of Geophysical Research* 67:4055–4061.

King T. V. V. and Ridley W. I. 1987. Relation of the spectroscopic reflectance of olivine to mineral chemistry and some remote sensing implications. *Journal of Geophysical Research* 92: 11457–11469.

King E. A., Jarosewich E., and Daughtery F. W. 1981. Tierra Blanca: An unusual achondrite from west Texas. *Meteoritics* 16:229–237.

Macgregor I. D. 1970. The effects of CaO, Cr_2O_3, Fe_2O_3, and Al_2O_3 on the stability of spinel and garnet peridotites. *Physics of the Earth and Planetary Interiors* 3:372–377.

Macgregor I. D. 1974. The system MgO-Al_2O_3-SiO_2: Solubility of Al_2O_3 in enstatite for spinel and garnet peridotite compositions. *American Mineralogist* 59:110–119.

Mao H. K. and Bell P. M. 1975. Crystal field effects in spinels: Oxidation states of iron and chromium. *Geochimica et Cosmochimica Acta* 39:865–874.

Mason B. 1963. The hypersthene achondrites. *American Museum Novitates* 2155:1–13.

Mason B., Nelen J. A., Muir P., and Taylor S. R. 1975. The composition of the Chassigny meteorite. *Meteoritics* 11:21–27.

Mattioli G. S. and Wood B. J. 1986. Upper mantle oxygen fugacity recorded by spinel-lherzolites. *Nature* 322:626–628.

Mattioli G. S. and Wood B. J. 1988. Magnetite activities across the $MgAl_2O_4$-Fe_3O_4 spinel join, with application to thermobarometric estimates of upper mantle oxygen fugacity. *Contributions to Mineralogy and Petrology* 98:148–162.

McSween H. Y., Jr. 1977. Carbonaceous chondrites of the Ornans type: A metamorphic sequence. *Geochimica et Cosmochimica Acta* 41:477–491.

Meteorite Working Group 1991. *Antarctic Meteorite Newsletter* 14: 19.

Mikouchi T., Chikami J., Takeda H., and Miyamoto M. 1995. Mineralogical study of LEW 88774: Not so unusual ureilite. Proceedings, 26th Lunar and Planetary Science Conference pp. 871–872.

Mukherjee A. B., Bulatov V., and Kotelnikov A. 1990. New high P-T experimental results on orthopyroxene-chrome spinel equilibrium and a revised orthopyroxene-spinel cosmothermometer. Proceedings, 20th Lunar and Planetary Science Conference. pp. 299–308.

Murck B. W. and Campbell I. H. 1986. The effects of temperature, oxygen fugacity, and melt composition on the behavior of chromite in basic and ultrabasic melts. *Geochimica et Cosmochimica Acta* 50:1871–1887.

Navrotsky A. and Kleppa O. J. 1967. The thermodynamics of cation distributions in simple spinels. *Journal of Inorganic and Nuclear Chemistry* 29:2701–2714.

Nell J. and Wood B. J. 1991. High-temperature electrical measurements and thermodynamic properties of Fe_3O_4-$FeCr_2O_4$-$MgCr_2O_4$-$FeAl_2O_4$ spinels. *American Mineralogist* 76: 405–426.

Nell J., Wood B. J., and Mason T. O. 1989. High-temperature cation distributions in Fe_3O_4-$MgAl_2O_4$-$MgFe_2O_4$-$FeAl_2O_4$ spinels from

thermopower and conductivity measurements. *American Mineralogist* 74:339–351.

Nicholls J. and Carmichael I. S. E. 1972. The equilibration temperature and pressure of various lava types with spinel- and garnet-peridotite. *American Mineralogist* 57:941–959.

Obata M. 1976. The solubility of Al_2O_3 in orthopyroxenes in spinel and plagioclase peridotites and spinel pyroxenite. *American Mineralogist* 61:804–816.

O'Neill H. St. C. and Navrotsky A. 1984. Cation distribution and thermodynamic properties of binary spinel solid solutions. *American Mineralogist* 69:733–753.

O'Neill H. St. C. and Wall V. J. 1987. The olivine-orthopyroxene-spinel oxygen geobarometer, the nickel precipitation curve, and the oxygen fugacity of the Earth's upper mantle. *Journal of Petrology* 28:1169–1191.

Pieters C. M. 1983. Strength of mineral absorption features in the transmitted component of near-infrared light: First results from RELAB. *Journal of Geophysical Research* 88:9534–9544.

Poole C. P. 1964. The optical spectra and color of chromium containing solids. *Journal of Physics and Chemistry of Solids* 25: 1169–1182.

Powell B. N. 1971. Petrology and chemistry of mesosiderites—II. Silicate textures and compositions and metal-silicate relationships. *Geochimica et Cosmochimica Acta* 35:5–34.

Preudhomme J. and Tarte P. 1971a. Infrared studies of spinels: I. A critical discussion of the actual interpretations. *Spectrochimica Acta* 27A:961–968.

Preudhomme J. and Tarte P. 1971b. Infrared studies of spinels: II. The experimental bases for solving the assignment problem. *Spectrochimica Acta* 27A:845–851.

Preudhomme J. and Tarte P. 1971c. Infrared studies of spinels: III. The normal II-III spinels. *Spectrochimica Acta* 27A:1817–1835.

Preudhomme J. and Tarte P. 1972. Infrared studies of spinels: IV. Normal spinels with a high-valency tetrahedral cation. *Spectrochimica Acta* 28A:69–79.

Prinz M., Klimentidis R., Harlow G. E., and Hewins R. H. 1978. Petrologic studies bearing on the origin of the Lodran meteorite (abstract). Proceedings, 9th Lunar and Planetary Science Conference. pp. 919–921.

Prinz M., Waggoner D. G., and Hamilton P. J. 1980. Winonaites: A primitive achondritic group related to silicate inclusions in IAB irons (abstract). Proceedings, 11th Lunar and Planetary Science Conference. pp. 679–680.

Prinz M., Weisberg M. K., Nehru C. E., and Delaney J. S. 1986. A second Brachina-like meteorite (abstract). Proceedings, 17th Lunar and Planetary Science Conference. pp. 679–680.

Prinz M., Weisberg M. K., and Nehru C. E. 1990. LEW 87051, a new angrite: Origin in a Ca-Al-enriched eucritic planetesimal? (abstract). Proceedings, 21st Lunar and Planetary Science Conference. pp. 979–980.

Rajan S. and Gaffey M. J. 1984. Spectral reflectance characteristics of Allende white inclusions (abstract). Proceedings, 15th Lunar and Planetary Science Conference. pp. 659–660.

Reed J. R. 1971. Optical absorption spectra of Cr^{3+} in $MgO{\cdot}Al_2O_3$-$MgO{\cdot}3.5Al_2O_3$ spinels. *Journal of American Ceramic Society* 54:202–204.

Reflectance Experiment Laboratory 1996. *Reflectance Experiment Laboratory (RELAB) description and user's manual.* Providence: Brown University.

Roeder P. L., Campbell I. H., and Jamieson H. E. 1979. A re-evaluation of the olivine-spinel geothermometer. *Contributions to Mineralogy and Petrology* 68:325–334.

Rossman G. R. 1988a. Vibrational spectroscopy of hydrous components. In *Reviews in mineralogy 18. Spectroscopic methods in mineralogy and geology,* edited by Hawthorne F. C. Washington D.C.: Mineralogical Society of America. pp. 193–206.

Rossman G. R. 1988b. Optical spectroscopy. In *Reviews in mineralogy 18. Spectroscopic methods in mineralogy and geology,* edited by Hawthorne F. C. Washington D.C.: Mineralogical Society of America. pp. 207–254.

Rossman G. R. and Smyth J. R. 1990. Hydroxyl contents of accessory minerals in mantle eclogites and related rocks. *American Mineralogist* 75:775–780.

Roush T. L., Singer R. B., and McCord T. B. 1985. Reflectance spectra of selected mafic silicates from .6 to 4.6 μm (abstract). Proceedings, 18th Lunar and Planetary Science Conference. pp. 854–855.

Rumble D., III. 1973. Oxide minerals from regionally metamorphosed quartzites of western New Hampshire. *Contributions to Mineralogy and Petrology* 42:181–195.

Sack R. O. 1982. Spinels as petrogenetic indicators: Activity composition relations at low pressure. *Contributions to Mineralogy and Petrology* 71:169–186.

Sack R. O. and Ghiorso M. S. 1991. Chromian spinels as petrogenetic indicators: Thermodynamics and petrological applications. *American Mineralogist* 76:827–847.

Schmetzer K. and Gübelin E. 1980. Alexandrite-like natural spinel from Sri Lanka. *Neues Jahrbuch fuer Mineralogie, Monatshefte* 9:428–432.

Sevastyanov B. K. and Orekhova V. P. 1971. Optical absorption spectrum of excited Cr^{3+} ions in $MgAl_2O_4$ spinel crystals. *Soviet Journal of Quantum Electronics* 1:91–97.

Shankland T. J., Duba A. G., and Woronow A. 1974. Pressure shifts of optical absorption bands in iron-bearing garnet, spinel, olivine, pyroxene, and periclase. *Journal of Geophysical Research* 79:3273–3282.

Shigley J. E. and Stockton C. M. 1984. "Cobalt-blue" gem spinels. *Gems & Gemology* 20:34–41.

Slack G. A. 1964. $FeAl_2O_4$-$MgAl_2O_4$: Growth and some thermal, optical, and magnetic properties of mixed single crystals. *Physical Review* 134:A1268–A1280.

Slack G. A., Ham F. S., and Chrenko R. M. 1966. Optical absorption of tetrahedral Fe^{2+} (3d6) in cubic ZnS, CdTe, and $MgAl_2O_4$. *Physical Review* 152:376–402.

Smith J. V. and Steele I. M. 1976. Lunar mineralogy: A heavenly detective story. Part II. *American Mineralogist* 61:1059–1116.

Smith M. R., Laul J. C., Ma M. S., Huston T., Verkouteren R. M., Lipschutz M. E., and Schmitt R. A. 1984. Petrogenesis of the SNC (shergottites, nakhlites, chassignites) meteorites: Implications for their origin from a large diverse planet, possibly Mars. *Journal of Geophysical Research* 89:B612–B630.

Sviridov D. T., Sevastyanov B. K., Orekhova V. P., Sviridova R. K., and Veremeichik T. F. 1973. Optical absorption spectra of excited Cr^{3+} ions in magnesium spinel at room and liquid nitrogen temperatures. *Optics and Spectroscopy* 35:59–61.

Takeda H., Saiki K., Otsuki M., and Hiroi T. 1993. A new Antarctic meteorite with chromite, orthopyroxene, and metal with reference to a formation model of S asteroids (abstract). Proceedings, 24th Lunar and Planetary Science Conference. pp. 1395–1396.

Taran M. N., Platonov A. N., Polshin E. V., and Matsuk S. S. 1987. Optical spectra and coloration of natural spinels of the (Mg, Zn, Fe)(Al, Fe)$_2O_4$ composition. *Mineralogicheskiÿ Zhurnal* 9:3–15.

Ulmer G. C. and White W. B. 1966. Existence of chromous ion in the spinel solid solution series $FeCr_2O_4$-$MgCr_2O_4$. *Journal of the American Ceramic Society* 49:50–51.

Wagner C. and Velde D. 1987. Aluminous spinels in lamproites: Occurrence and probable significance. *American Mineralogist* 72:689–696.

Webster R. 1983. *Gems: Their sources, descriptions and identification, Fourth edition.* London: Butterworths.

White W. B. and DeAngelis B. A. 1967. Interpretation of the vibrational spectra of spinels. *Spectrochimica Acta* 23A:985–995.

Wood B. J., Kirkpatrick R. J., and Montez B. 1986. Order-disorder phenomena in $MgAl_2O_4$ spinel. *American Mineralogist* 71:999–1006.

Wood D. L., Imbusch G. F., Macfarlane R. M., Kisliuk P., and Larkin D. M. 1968. Optical spectrum of Cr^{3+} ions in spinels. *Journal of Chemical Physics* 48:5255–5263.

Woodland A. B. and Wood B. J. 1990. The breakdown of hercynite at low fO_2. *American Mineralogist* 75:1342–1348.

Yugami K., Takeda H., Kojima H., and Miyamoto M. 1996. Distribution of opaque minerals in primitive achondrites (abstract). Proceedings, 27th Lunar and Planetary Science Conference. pp. 1483–1484.